STUDY OF SECOND-ORDER TURBULENCE CLOSURE TECHNIQUE AND ITS APPLICATION TO ATMOSPHERIC FLOWS

by PIOTR J. FLATAU

Atmospheric Science
PAPER NO.
393

US ISSN 0067-0340

DEPARTMENT OF ATMOSPHERIC SCIENCE
COLORADO STATE UNIVERSITY
FORT COLLINS, COLORADO

STUDY OF SECOND-ORDER TURBULENCE CLOSURE TECHNIQUE AND ITS APPLICATION TO ATMOSPHERIC FLOWS

by

Piotr J. Flatau

Research supported by the

Air Force Geophysics Laboratory
under Contract #F19628-84-C0005

and by

the Electric Power Research Institute
under Contract #RFP 1630-25

Department of Atmospheric Science
Colorado State University
Fort Collins, Colorado

Atmospheric Science Paper No. 393

ABSTRACT

STUDY OF SECOND-ORDER TURBULENCE CLOSURE TECHNIQUE
AND ITS APPLICATION TO ATMOSPHERIC FLOWS

The applicability of the second-order turbulence closure technique to atmospheric mesoscale flows is investigated. Analytical and numerical studies of various closure schemes are performed. Theoretical investigations of the well-known Mellor and Yamada approach result in new realizability conditions for the Level 2.5 and Level 3.0 schemes.

The bulk parameters (eddy exchange coefficients) are calculated from the full second order closure model. The comparison of these parameters with the experimental data reveals that the simple Richardson number-based scaling is not adequate.

The Level 2.5 and Level 4.0 models are developed and applied to a California stratocumulus case. The new realizability conditions are applied in the Level 2.5 model. The results are presented and show good agreement with experimental data collected off the California shoreline.

On the basis of these studies, conclusions about applicability of simplified second-order turbulence closure technique are formulated.

Piotr J. Flatau
Department of Atmospheric Science
Colorado State University
Fort Collins, Colorado 80523
Fall 1985

ACKNOWLEDGEMENTS

I would like to express my appreciation to Professor William R. Cotton, my thesis advisor, for his support, encouragement, and many helpful suggestions throughout the course of this research. I would like to thank Professor K. Haman whose determination made my trip to CSU possible. He was my first teacher of atmospheric science.

I especially appreciate the numerous discussions, arguments, comments, help and kindness of Dr. Chaing Chen. I made his life miserable for several months while learning details of his model. Chaing's expertise and willingness to help with problems contributed greatly to the modelling portions of this study.

I also thank Dr. Wayne H. Schubert, member of my graduate committee, for many hours of most useful conversations on almost all aspects of atmospheric science. All I know about experimental measurements of turbulent flows is due to the other member of my graduate committee, Professor Virgil A. Sandborn. Several conversations and letters exchanged with Dr G.L. Mellor were very useful.

I would like to express my appreciation to other members of our research group at Colorado State University - Jerry Schmidt, Greg Tripoli, Craig Tremback, Ray McAnelly, Brenda Thompson, Kevin Knupp, Jack Lin, Sue Chen, and others who contributed substantially and in different ways to this project.

Finally, I would like to express my gratitude to my friend, Annette Claycomb, who tried to translate my polglish into English.

This research was supported by the Air Force Geophysics Laboratory, Meteorology Division - Cloud Physics Branch under Contract #F19628-84-C-0005 and under Electric Power Research Institute Contract #RFP 1630-25. Computations were performed on the National Center for Atmospheric Research (NCAR) Cray-1 computer. NCAR is supported by the National Science Foundation.

TABLE OF CONTENTS

LIST OF SYMBOLS

Symbol	Explanation
A_1, A_2	Empirical constants = (0.92, 0.74)
B_1, B_2	Empirical constants = (16.6, 10.1)
C_1	Empirical constant = 0.08
$\overline{ab}$	Turbulent covariance of two scalars a and b
c_p	Specific heat capacity of air at constant pressure
c_v	Specific heat capacity of air at constant volume
f	Coriolis parameter
F	Total radiation flux
g	Acceleration of gravity
G_H	Non-dimensional parameter related to the mean potential temperature gradient
G_M	Non-dimensional parameter related to the mean velocity gradient
G_T	Non-dimensional parameter related to potential temperature variance
k	von Karman constant
K_H	Eddy exchange coefficient for scalar quantities
K_M	Momentum eddy exchange coefficient
l	Turbulent length scale
l_1, l_2	Length scales = $(A_1, A_2)l$
L	Monin-Obukhov length

p	Pressure
P_b	Turbulent buoyancy production
P_s	Turbulent shear production
R_d	Gas constant of dry air
R_f	Flux Richardson number
R_{fc}	Critical (flux) Richardson number
R_i	Bulk Richardson number
r_c	Mixing ratio of cloud water
r_l	Mixing ratio of liquid water
r_r	Mixing ratio of rain water
r	Mixing ratio of total water
r_v	Mixing ratio of water vapor
S_H	Non-dimensional scalar eddy exchange coefficient
S_M	Non-dimensional momentum eddy exchange coefficient
$\overline{q^2}$	Turbulent kinetic energy
t	Time
T	Temperature
u,v,w	x,y and z components of velocity
u_i	i-component of velocity
u_g, v_g	Geostrophic wind components
u_*	Friction velocity
$\overline{u_i u_k}$	Reynolds stress covariances
$\overline{u_i a}$	Velocity-scalar covariance
$\overline{u^2}$	u-velocity variance
θ	Potential temperature
θ_o	Basic state potential temperature
θ_{il}	Ice water potential temperature

θ_v	Virtual potential temperature
ρ_o	Basic state density
α	Ratio of velocity gradients
β	Inverse of basic state potential temperature
ε	Turbulent dissipation
Λ_1, Λ_2	Length scales = $(A_1, A_2)l$

1. INTRODUCTION

The purpose of this research is to investigate the applicability of the second-order turbulence closure technique to atmospheric mesoscale flows. Specifically, it attempts to contribute to understanding just how well the simplified second-order schemes describe such flows. To accomplish this objective (at least partially) we performed a numerical and analytical study of Zeman and Lumley (1976) and Mellor and Yamada (1982) closures. This goal is related to the ongoing research at our CSU group on development of Regional Atmospheric Modeling System (RAMS).

1.1 Statement of the Problem

The RAMS model is being applied to a variety of atmospheric phenomena such as study of three-dimensional, non-hydrostatic cumulonimbus development, mountain flows, one-dimensional stratocumulus research, and large eddy turbulence simulations. The turbulence is important in most mesoscale flows. It provides a mechanism for momentum, heat, and moisture transport. It interacts and modifies the meteorological fields such as winds, temperature, solar radiation, and cloud droplets. Different scales are involved, ranging from the turbulent enhancement of cloud droplet coagulation, to radiative-turbulent entrainment processes at the top of cloud layers, to growing planetary boundary layers on hot days. These different scales have to be filtered depending on the problem at hand--resulting in more or less simplified schemes (parameterization). Several methods to study and parameterize atmospheric turbulence have been proposed. These are

direct solution of Navier-Stokes equations, higher order closure models and mixed layer models. We concentrate here on second-order closure techniques since their intermediate complexity makes them feasible for use in mesoscale models with the current generation of computers. There is now a growing understanding that the approaches to the turbulence parameterization should be complementary. For example, the large eddy simulation (LES) which is the solution to the Navier-Stokes equations on three-dimensional, high resolution grids may provide closure constants for the Reynolds averaged equations. On the other hand, the Reynolds averaged turbulence equations are used to parameterize sub-grid turbulence in LES models. The mixed layer schemes, used now almost exclusively in the Global Circulation Models, can be tuned on the basis of the higher level closure results (entrainment rate, time rate of the PBL growth, etc.) The above examples are just a few. In our group we use the second-order closure to model the sub-grid fluxes in the LES model. The problem which arose very early in that project was the magnitude of the sub-grid eddy exchange coefficients. They were changed, but the problem of how to justify these changes on the basis of the implemented model remains unsolved. Recently another problem, namely the parameterization of the stratiform clouds in mesoscale models, occurred in conjunction with the modeling of weather modification in the California region. We will use mixed layer or low resolution second-order closure model approach but the understanding of the physical mechanisms governing California stratus as seen through the detailed second-order closure model is certainly helpful.

After expressing our belief that we deal with a well-posed problem we then describe what we have done to solve it. Chapter 2 is devoted to

the model description used and studied in this thesis. We describe the hierarchy of models (classified there according to the Mellor and Yamada scheme) and perform some algebraic manipulations on the basic set of equations. This chapter introduces the basic notation and contains standard material. In Chapter 3 we study analytically Mellor and Yamada's simplified schemes (Level 2.0, 2.5 and 3.0). Some new results are described, and they are related to the so-called realizeability conditions, i.e. limits of model validity. We discuss the local equilibrium assumption and its applicability, and the role of the diffusional terms is investigated. In Chapter 4 we compare Chen and Cotton's level 3.5 model with the more simplified second-order scheme. The experimental results on eddy exchange coefficients are discussed there. We try to estimate what the limits of the simplified schemes are and why they miss some of the physics. In Chapter 5 some numerical studies are presented. The levels 2.5 and 4 are used to simulate a California stratus case. In the last Chapter, summary and conclusions are provided.

2. MODEL EQUATIONS

In this chapter we provide the mathematical description of the physical phenomena we try to analyze. First the mean flow (Navier-Stokes) equations for the horizontally-homogeneous atmospheric mixed layer are written. Then we briefly describe the physical processes we are able to capture, at least in an approximate way, in the model. Finally we deal in detail with the turbulence parameterization. Extensive algebra is used to describe levels of turbulence parameterization, but the concepts are simple.

2.1 Mean Flow Equations

This model is in many respects a continuation and modification of the effort of Cotton's group to develop a multipurpose mesoscale modeling system. Therefore most of the dynamics and physics are taken as is from the RAMS model. In particular what follows in this paragraph is a summary of an excellent and detailed description given by Chen in his thesis (1984).

A model of a horizontally-homogeneous mixed layer can be described by the following ensemble-averaged equations.

$$\frac{\partial \bar{u}}{\partial t} = f\bar{v} - f\overline{v_g} + \frac{\partial}{\partial z}\left(-\overline{u''w''}\right) - \bar{w}\frac{\partial \bar{u}}{\partial z} \tag{2.1}$$

$$\frac{\partial \bar{v}}{\partial t} = -f\bar{u} + f\overline{u_g} + \frac{\partial}{\partial z}\left(-\overline{v''w''}\right) - \bar{w}\frac{\partial \bar{v}}{\partial z} \tag{2.2}$$

$$\frac{\partial \bar{\theta}_{il}}{\partial t} = -\bar{w}\frac{\partial}{\partial z}\bar{\theta}_{il} - \frac{\partial}{\partial z}\left(\overline{-w''\theta_{il}''}\right) - \frac{1}{\rho_o c_p}\frac{\partial F}{\partial z} - \bar{\theta}\frac{L_{lv}}{c_p}\,PR_r/\max(T,253) \tag{2.3}$$

$$\frac{\partial \bar{r}}{\partial t} = -\bar{w}\frac{\partial}{\partial z}\bar{r} - \frac{\partial}{\partial z}\left(\overline{w''r''}\right) + PR_r \tag{2.4}$$

$$\frac{\partial \bar{r}_r}{\partial t} = -\bar{w}\frac{\partial}{\partial z}\bar{r}_r - \frac{\partial}{\partial z}\left(\overline{w''r_r''}\right) + CN_{cr} + AC_{cr} - VD_{rv} + PR_r \tag{2.5}$$

where the variables $(\bar{u},\bar{v},\bar{w})$ are the ensemble-averaged wind components in the (x,y,z) direction. The variables $(\bar{u}_g,\bar{v}_g)$ are the geostrophic wind components in the (x and y) direction. The Coriolis parameter is represented by f. The atmospheric radiative cooling or heating rate is represented by the radiational flux divergence $(-(1/\rho_o c_p)\,(\partial F/\partial z))$. F is the total radiation flux defined by $F = F\uparrow - F\downarrow$ where $F\uparrow$ and $F\downarrow$ represent upward and downward flux, respectively. The ρ_o is the reference state air density. Equations (1) and (2) can be derived from the equations of motion. In the derivation, the velocity field is decomposed into ensemble-averaged mean and perturbation. $u_i = \bar{u}_i + u_i''$ where u_i'' represents the fluctuations from the ensemble average. The thermodynamic variables can also be decomposed into $\theta_{il} = \bar{\theta}_{il} + \theta_{il}''$; $r = \bar{r} + r''$, where θ_{il} and r are ice-liquid water potential temperature and total water mixing ratio, respectively. A double superscript prime notation is used for turbulent fluctuations.

The rain water mixing ratio and its turbulence fluctuation are represented by $\bar{r}_r$ and r_r'' . The microphysical processes, such as auto conversion, accretion, evaporation and precipitation are represented by CN_{cr}, AC_{cr}, VD_{rv} and PR_r. The subscripts c, r and v denote cloud water, rain water and vapor.

2.2 Model Physics

In the previous paragraph we wrote the basic equations for the mean flow quantities. There are several physical processes taken into account in the model. These are radiation, cloud microphysics, sub-grid condensation scheme, and turbulence.

The radiation model consists of two parts: short-wave and long-wave radiation. The parameterization of long-wave radiation flux through a clear atmosphere follows Rodgers (1967); for a cloudy atmosphere, Stephens' (1978a,b) parameterization is used. This parameterization is based on the 'effective' emissivity of the cloud. For the emissivity of an air column containing a clear and cloudy atmosphere (or a partially cloudy atmosphere), Herman and Goody's (1976) 'mixed-emissivity' assumption is adopted.

The short-wave radiation model includes atmospheric molecular scattering, Lacis and Hansen's (1974) ozone absorption, and Stephens' (1978b) parameterization of reflectance, transmittance, and absorptance of a cloud layer. The structure of the short-wave radiation model follows that of Stephens and Webster (1979), which is a two-stream model (upward and downward flux). Stephens' (1977) 'equivalent transmittance' is employed to derive the reflectance, transmittance and absorptance of a 'clear-cloud mixed' atmosphere.

Thermodynamical processes (Tripoli and Cotton,1982) include use of ice-liquid water potential temperature $\overline{\theta_{il}}$. The cloud microphysics (bulk parameterization) include the diagnosis of cloud water, rain water and water vapor (ice processes are parameterized, they but are not used here).

A partial condensation scheme (Banta,1980) is used to diagnose cloud water and cloud water co-variances.

2.3 Hierarchy of Turbulence Models

In a sequence of papers, Mellor and Yamada (Mellor,1973,1977; Mellor and Yamada,1974,1982; Yamada,1975,1983; Yamada and Mellor,1979) (hereafter refered to as M-Y) developed the hierarchy of models based on the second-order closure approach. A different degree of simplification was employed, and the resulting scheme was defined as a level. Initially four levels were introduced (Level 4 the most complex and Level 1 the simplest), but soon it became apparent that this classification was too narrow, and now we have levels 1.0, 1.5, 2.0, 2.5, 3.0, 3.5 and 4. And there are even hybrids of different levels , e.g. 2 and 2.5. This section discusses different levels of the second-order turbulence closure. We will describe here the full model and then start to define simplified schemes. But we begin with the Chen and Cotton (1983) (hereafter refered to as CC) implementation of the second order closure because this was the foundation turbulence model of our group and we performed some initial experiments on it (Chapter 4).

In a sequence of papers Zeman and Lumley (1976) (ZL) developed a model based on the second-order closure technique. This approach was found particularly useful for the study of turbulence in clouds and was adopted by CC. CC extended ZL closure scheme to include moist

processes. The CC model is almost a full implementation of the second-order turbulence parameterization. The authors call their model Level 3.5 second-order closure. It is 0.5 less than 4.0 because some of the co-variances are not prognostic but diagnostic. But in fact the largest difference between ZL and M-Y schemes lies in the assumptions about the diffusional third order terms. Their (ZL and CC) scheme may transport second-order turbulence quantities in the up-gradient way. This is believed to be important for the correct modeling of the buoyancy effects. The success of ZL and CC in predicting flows where buoyancy enhancement is important (e.g. at the top of the cloud layer) shows that ZL approach is valuable.

A problem we faced was application of the turbulent model to the large mesoscale model developed by Cotton's group at CSU. For mesoscale applications the turbulence sub-programs should be time and computer core efficient. This requires a reduction of the number of prognostic equations. At the same time, one would like to retain some of the predictions of turbulent quantities, such as turbulent kinetic energy (TKE). In this way the mechanism for advection of TKE would exist, i.e. the turbulence generation would not only be a local phenomenon. M-Y scheme seemed to be suitable for the above-mentioned goal, and we decided to implement their scheme.

The ZL and M-Y schemes are similar. In Appendix A we show how ZL model constants are related to the M-Y constants. The rest of this thesis follows M-Y notation, and even when we used the Z-L model we provided numerical values in terms of the M-Y scheme. Using results given in Appendix A we can easily convert them to ZL constants.

2.3.1 Level 4 - Full implementation of the second-order closure

The Reynolds-averaged equations for the Reynolds stress can be written as

$$\frac{\partial \overline{u_i u_k}}{\partial t} = P_{ik} + G_{ik} + S_{ik} - \Pi_{ik} - D_{ik}, \tag{2.6}$$

where P_{ik} and G_{ik} represent the mechanical production of $\overline{u_i u_k}$ by the vertical shear of $\overline{U_i}$ and the buoyancy production terms, respectively. The third-order correlation term is denoted as S_{ik} and the pressure-velocity correlation term by Π_{ik} . The dissipation term is D_{ik} . The equation for the turbulent covariances of arbitrary scalar quantities (a) such as $\overline{\theta_{il}}$, $\overline{r}$ and $\overline{r_r}$ with the velocity components is

$$\frac{\partial \overline{u_i a}}{\partial t} = A_{ia} + P_{ia} + G_{ia} + S_{ia} - \Pi_{ia} + PA(\overline{wa}) + S(\overline{wa}) \tag{2.7}$$

where A_{ia} represents advection, P_{ia} is a production term, G_{ia} is a dissipation term, S_{ia} is a triple correlation term and Π_{ia} is pressure-thermodynamic covariance. The $PA(\overline{u_i a})$, $S(\overline{u_i a})$ are rain/cloud water covariance terms.

Note that for the one-dimensional model, only derivatives with respect to z are non-zero. The Coriolis force has been neglected.

The equation for the turbulent covariances of two scalar quantities is given by

$$\frac{\partial \overline{ab}}{\partial t} = A_{ab} + P_{ab} + S_{ab} - D_{ab} + PA(\overline{ab}) + S(\overline{ab}) \tag{2.8}$$

where the notation similiar to that for the equation (2.7) is used. Equations (2.6-8) represent a full second-order closure (Level 4) model. We provide more complete discussion of this level in Appendix B1.

2.3.2 Level 3 and 2.5 models. Scaling analysis in terms of departure from isotropy parameter.

M-Y use departure from the isotropy as a small parameter in their analysis of the Reynolds equations. They show that in the atmospheric boundary layer (ABL) one can neglect diffusion, time and advection terms. Level 3 predicts only variances. In Level 2.5 only the equation for the turbulent kinetic energy (TKE) is retained. In Appendix B2 the final set of equations is shown both for the level 3.0 and for the level 2.5.

This is the set of twenty equations and twenty unknowns. In the dry case the amount of unknowns and equations reduces to ten. Because the system is linear it can be solved. The algebra is extensive; for many algebraic manipulations in this thesis we used the symbolic algebra program REDUCE 3 (Hearn,1984). We will show results for the calculations of the dry case. The extension to moist case is relatively simple.

To make the final formula more compact, let us introduce several non-dimensional quantities. The non-dimensional eddy exchange coefficients S_M and S_H are defined by the following equations

$$K_M = lqS_M \,, \tag{2.9}$$

$$K_H = lqS_H \,. \tag{2.10}$$

where K_M and K_H are momentum and heat eddy exchange coefficients, l is turbulent length scale, and q is defined by

$q^2 = \overline{u^2} + \overline{v^2} + \overline{w^2}$

We also define the non-dimensional parameters G_M, G_H, G_T and α, which are related to the mean flow variables

$$G_M = \frac{l^2}{q^2}\left(\left(\frac{\partial \bar{U}}{\partial z}\right)^2 + \left(\frac{\partial \bar{V}}{\partial z}\right)^2\right) = \frac{l^2}{q^2} S \tag{2.11}$$

$$G_H = -\frac{l^2}{q^2} \beta g \frac{\partial \bar{\theta}}{\partial z} \tag{2.12}$$

$$G_T = \frac{l^2}{q^2} \frac{(\beta g)^2}{q^2} \theta^2 \tag{2.13}$$

$$\alpha = \left(\frac{d\bar{U}}{dz}\right)^2 / \left[\left(\frac{d\bar{U}}{dz}\right)^2 + \left(\frac{d\bar{V}}{dz}\right)^2\right] \tag{2.14}$$

where $\beta = 1/\theta_o$. It can be seen that $0 \leq \alpha \leq 1$. Notice that G_M, G_H, G_T and α are related to the prognostic equations in the model. In other words, if we express all variables in terms of G_M, G_H, G_T and α, then the problem is solved. After some algebra we can show that S_M and S_H for the Level 3.0 are given by

$$S_M = \frac{S_M^n}{S^d},$$

$$S_H = \frac{S_H^n}{G_H S^d} \tag{2.15a,b}$$

where

$$S_M^n = 9G_H A_2 A_1 (A_2 + 4A_1 C_1) + A_1 (27A_1^2 G_T + 36A_2 A_1 G_T - 3C_1 + 1)$$

$$S_H^n = -9G_H^2 A_2^2 A_1 + 18G_H G_M A_2 A_1^2 C_1 + G_H A_2 (-27A_2 A_1 G_T + 1) + 18G_M A_2 A_1^2 G_T + 3A_2 G_T$$

$$S_d = 108G_H^2 A_2^2 A_1^2 + 54G_H G_M A_2^2 A_1^2 - 21G_H A_2 A_1 + 6G_M A_1^2 + 1 \tag{2.16a,b,c}$$

These formulas are the same as those in Mellor and Yamada's (1974) paper

(eqs 55,56), although they are written here in the non-dimensional form.

For the Level 2.5 we get the non-dimensional eddy exchange coefficients in the form

$$S_M = \frac{S_M^n}{S^d},$$

$$S_H = \frac{S_H^n}{S^d} \qquad (2.17a,b)$$

where

$$S_d = (3G_H B_2 A_2 + 12G_H A_2 A_1 - 1)(6G_M A_1^2 - 9G_H A_2 A_1) - G_M G_H (54A_2^2 A_1^2 + 72A_2 A_1^3) + G_H A_2 (3B_2 + 12A_1) - 1$$

$$S_H^n = -(18G_M C_1 A_1^2 - 9G_H A_2 A_1 + 1)A_2$$

$$S_M^n = -G_H A_1 (9C_1 B_2 A_2 + 36C_1 A_2 A_1 - 3B_2 A_2 + 9A_2^2 - C_1 + 1)$$

For both levels the final set of equations is

$$\overline{u^2}/q^2 = 1/3 + A_1 \delta S_M G_M - 2A_1 S_H G_H,$$

$$\overline{v^2}/q^2 = 1/3 + A_1 \beta S_M G_M - 2A_1 S_H G_H,$$

$$\overline{w^2}/q^2 = 1/3 + 2A_1 S_M G_M + 4A_1 S_H G_H, \qquad (2.18a,b,c)$$

where $\delta = 2(3\alpha - 1)$ and $\beta = 2(2 - 3\alpha)$.

$$\overline{uv} = 6A_1 l^2 S_M \frac{\partial \bar{U}}{\partial z}\frac{\partial \bar{V}}{\partial z}$$

$$\overline{uw} = -lqS_M \frac{\partial \bar{U}}{\partial z}$$

$$\overline{vw} = -lqS_M \frac{\partial \bar{V}}{\partial z} \qquad (2.19a,b,c)$$

$$\overline{u\theta} = 3A_2 l(S_H + S_M) \frac{\partial \bar{\Theta}}{\partial z}\frac{\partial \bar{U}}{\partial z}$$

$$\overline{v\theta} = 3A_2 l(S_H + S_M) \frac{\partial \bar{\theta}}{\partial z} \frac{\partial \bar{V}}{\partial z}$$

$$\overline{w\theta} = -lqS_H \frac{\partial \bar{\theta}}{\partial z} \qquad (2.20a,b,c)$$

and for Level 2.5 only

$$\overline{\theta^2} = B_2 l S_H \frac{\partial \bar{\theta}}{\partial z} \qquad (2.21a)$$

The ratio of TKE production to dissipation can be expressed as

$$(P_s + P_b)/\varepsilon = B_1(S_M G_M + S_H G_H) \qquad (2.22a)$$

2.3.3 Level 2 - Local equilibrium assumption

The final assumption made by M-Y is that of local equilibrium. It states that local production of TKE is balanced by dissipation. The resulting model is completely diagnostic. Again we have the set of linear equations to solve, but further simplifications are possible. From the definition of the flux Richardson number

$$R_f = - P_b/P_s \qquad (2.23)$$

and local equilibrium hypothesis

$$P_s + P_b = \varepsilon \qquad (2.24)$$

we can show that

$$G_M = \frac{-1}{B_q S_M (R_f - 1)} \qquad (2.25)$$

and

$$G_H = \frac{R_f}{B_1 S_H (R_f - 1)} \tag{2.26}$$

Expressions for G_M and G_H depend on R_f, S_M and S_H only. Substitution into the linear set of equations (Appendix B) and solving for S_M and S_H gives

$$S_M = S_M (R_f),$$

and

$$S_H = S_H (R_f).$$

i.e., only one non-dimensional parameter, R_f, describes the mean flow state. In more explicit form, we can write the solution for the level 2 model as

$$S_H = \frac{A_H}{B_H} \frac{R_f - R_{f2}}{R_f - R_{f1}}, \tag{2.27}$$

and

$$S_M = \frac{A_M}{B_M} \frac{R_f - R_{f4}}{R_f - R_{f3}}, \tag{2.28}$$

where

$$\begin{aligned} A_H &= A_2 (3 B_2 + B_1 + 12 A_1), \\ B_H &= B_1, \\ A_M &= A_1 (-3 C_1 B_1 + B_1 + 9 A_2 12 A_1), \\ B_M &= A_2 (3 B_2 + B_1 + 3 A_1), \end{aligned} \tag{2.29}$$

and

$$R_{f1} = 1,$$

$$R_{f2} = R_{fc} = \frac{B_1 - 6\,A_1}{3\,B_2 + B_1 + 12\,A_1},$$

$$R_{f3} = \frac{B_1 - 6\,A_1}{3\,B_2 + B_1 + 3\,A_1},$$

$$R_{f4} = \frac{3\,C_1B_1 - B_1 + 6\,A_1}{3\,C_1B_1 - B_1 - 9\,A_2 - 12\,A_1}. \qquad (2.30)$$

3. ANALYTICAL RESULTS FOR THE MELLOR AND YAMADA HIERARCHY OF MODELS

In this chapter we discuss some analytical results and realizabilty conditions for the Mellor and Yamada (1982) hierarchy of models. We will proceed from the simplest, Level 2.0 scheme up to the Level 4. The purpose of such a study is to decide what the possible limitations of the scheme are. Using the typical values of parameters G_H, G_M, G_T, R_f and α (see Chapter 2), we are able to plot fields of turbulent variances and co-variances. Obvious criteria such as positive-definiteness of variances are used to limit the possible range of mean flow values.

3.1 Level 2

The one-parameteric M-Y Level 2 functions are simple to deal with. An asymptotic analysis shows that for very unstable conditions (large $-R_f$), S_H and S_M tend to constant values

$$S_{H\infty} = \frac{A_H}{B_H}, \tag{3.1}$$

$$S_{M\infty} = \frac{A_M}{B_M}\frac{A_H}{B_H}, \tag{3.2}$$

and

$$\alpha_\infty = \frac{S_{H\infty}}{S_{M\infty}} = \frac{B_M}{A_M}. \tag{3.3}$$

The last quantity is the inverse of turbulent Prandtl number.

Both S_M and S_H go to zero for $R_f = R_{f2}$, and we interpret this value as a critical Richardson number R_{fc}. Inverse Prandtl number

$$\alpha = \frac{S_H}{S_M} = \frac{B_M}{A_M} \frac{R_f - R_{f3}}{R_f - R_{f4}}$$

goes to zero for $R_f = R_{f3}$.

Figs. 3.1a,b,c,d show eddy exchange coefficients S_H, S_M and the ratio S_H/S_M for the constants A_1, A_2, B_1, B_2, C_1, C_2, and C_3 defined in M-Y and ZL works (see Appendix A). Also, sensitivity of results to changes in C_1 is presented. Fig. 3.1a shows the M-Y case with the constants as determined in their 1982 paper. The critical Richardson number is $R_{fc} = 0.19$. This is in good agreement with other theoretical studies. Both S_H and S_M tend to constant values in the very unstable region - $S_{H\infty} = 2.58$ and $S_{H\infty} = 1.96$.

Values of the inverse of the turbulent Prandtl number $\alpha = S_H/S_M$ are also plotted. This can be directly compared with the experimental results obtained by Ueda (1981) (see next chapter). Ueda's results approach 1 at $R_i = -10$ (Fig. 4.4). The M-Y model gives a value close to 1.3 (Fig. 3.1a, curve c). In the surface layer, observations show that the ratio K_H/K_M continues to increase with increasing instability. Here the constant value $S_{H\infty}/S_{M\infty}$ is attained in partial agreement with Ueda's (1981) data. Fig. 3.1b shows the same data for $C_1 = 0$. This coefficient is related to the rapid term in the parameterization of the pressure-velocity covariances. The results are sensitive to such a change. In particular, in the stable regime the S_M becomes larger than S_H.

Results based on ZL parameterization constants (Appendix A) are shown on Figs. 3.1c,d. In general, they exhibit the same behavior as in

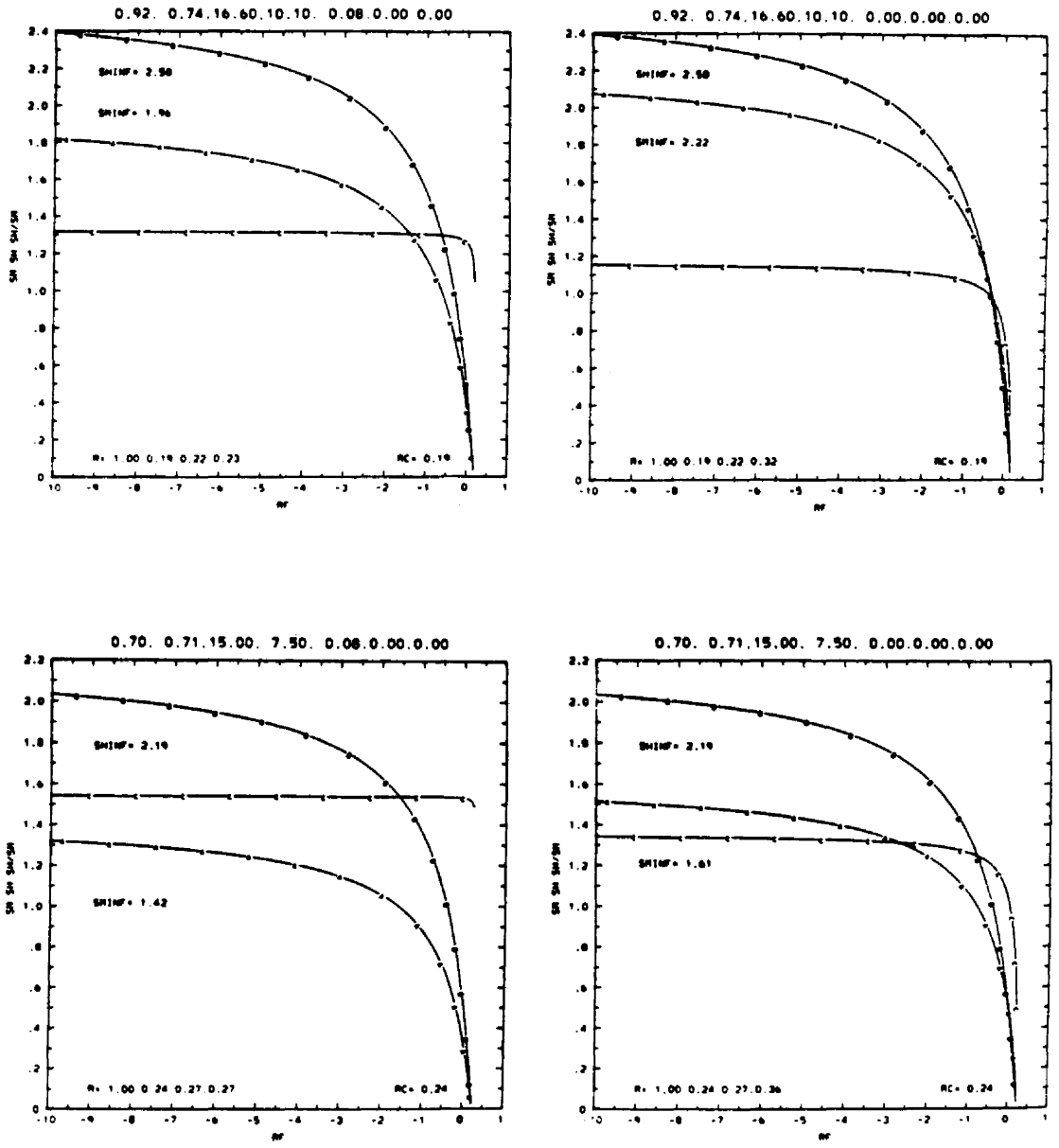

Fig. 3.1. Level 2 eddy exchange coefficients as a function of the flux Richardson number S_M (curve A), S_H (curve B) and the inverse Prandtl number (curve C). Critical Richardson number is indicated by RC. Asymptotic values of S_H and S_M (for very large and negative R_f) are given by SHINF and SMINF. Constants of parameterizations - A_1, A_2, B_1, B_2, C_1, C_2 are at the top of the plot. (a) M-Y, (b) M-Y, C_1 = 1, (c) ZL , (d) ZL, C_1 = 1.

the M-Y case. The critical flux Richardson number is $R_{fc} = 0.24$. Limiting values for S_H and S_M are 2.19 and 1.42, respectively. Fig. 3.1d presents data for $C_1 = 0$. Again S_M is larger than S_H in the stable region. The sensitivity test for C_1 in ZL's case is of some importance. CC assumed, after ZL, that $C_1 = 0$. This eliminates the mean wind shear contribution to the pressure velocity covariance.

ZL set $C_1 = 0$ because they investigated flows in stratified fluid without the mean shear. In general $C_1 \neq 0$, particularly for cases with large mean wind gradients. We ran a test with $C_2 = 0.2$. This value was suggested by Zeman (1975). The results (not shown here) give large deviations from the experimental data, particularly for the stable and weakly unstable regions.

In conclusion, the results are sensitive to changes in parameterization constants, but they compare satisfactorily with some of the experimental data.

3.2 Level 2.5

We will proceed now to the description of the level 2.5 functions. We release assumption about local equilibrium $P_s + P_b = \varepsilon$ and have a model where three parameters are important. These are G_H (non-dimensional temperature gradient), G_M (non-dimensional quantity related to the mean flow shear) and α (ratio of shear squares in the x and y directions). See Chapter 2 for their definitions. The contours of turbulent quantities such as non-dimensional momentum and heat eddy coefficients, turbulent variances $\overline{u^2}$, $\overline{v^2}$, $\overline{w^2}$ and ratio of the turbulent production to the turbulent dissipation are plotted here with G_H and G_M as independent variables. The α-dependence of these turbulent quantities will be also discussed.

Let us start with the Figs. 3.3b where $(P_s + P_b)/\varepsilon$ is plotted. The G_M values are always positive and are shown there for (0.,3.) region. The G_H values can be negative (for stable case) and positive (for unstable case). The (-0.4,0.1) range of G_H values is used here. The isoline $(P_s + P_b)/\varepsilon = 1$ corresponds to the local equilibrium assumption. On the other hand, for arbitrary G_H and G_M the $(P_s + P_b)/\varepsilon \neq 1$. This is clearly seen in Fig. 3.3b. In Fig. 3.3b isolines labeled INF-1 represent values of G_H and G_M for which $(P_s + P_b)/\varepsilon$ is singular. Curves labeled P1 and P2 give G_H and G_M values where $(P_s + P_b)/\varepsilon$ goes to zero. Contours are plotted for $(P_s + P_b)/\varepsilon = (0.5,1.0,1.5,2.0,2.5)$.

The P1 isoline originates at $G_M = 0$ and $G_H = 0$. It delimits the region of positive (upper part) and negative (lower part) values of $(P_s + P_b)/\varepsilon$. For the stable case ($G_H < 0$) and small G_M, the buoyancy term P_b becomes negative and is larger than shear generation term P_s. This leads to negative $(P_s + P_b)/\varepsilon$. On the other hand, for the unstable case, values of $(P_s + P_b)/\varepsilon$ are always positive.

Figs. 3.2 and 3.3a present values of eddy exchange coefficients S_M and S_H. The INF-1 curve is the same as before and represents G_H and G_M values for which S_H and S_M tends to infinity. These large values of exchange coefficients are not physically possible and the region close to the INF curve has to be somehow excluded. The values to the left of INF curve are positive which indicates positive exchange coefficients. On the S_M diagram the SM curve is for $S_M = 0$. In the region between INF and SM curves in Fig. 3.2, the S_M values are negative: however, from other considerations (positive definitness of velocity variances), we will have to exclude this region. In other words, Level 2.5 is forced to predict positive (down-gradient) values of exchange coefficients.

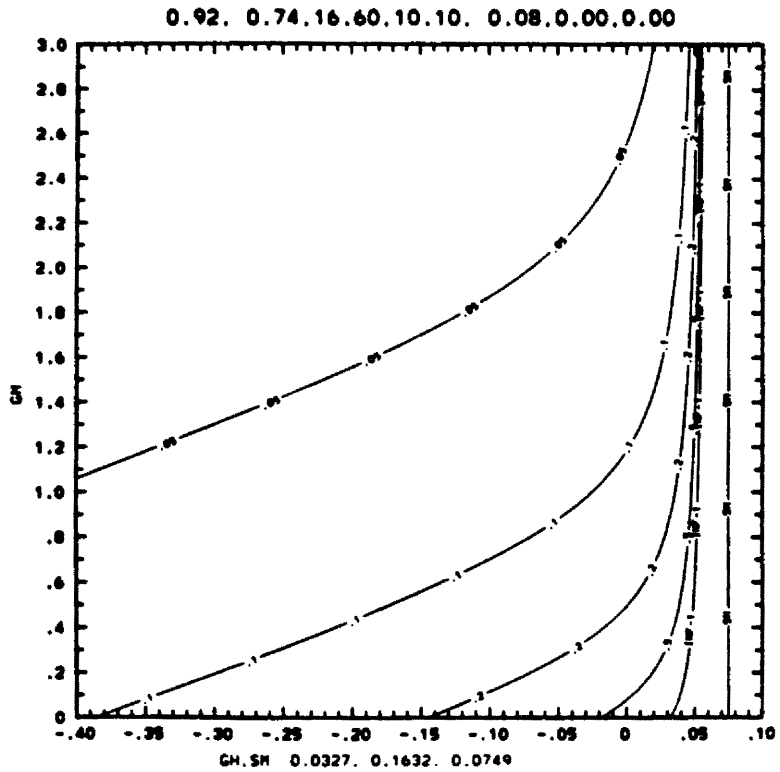

Fig. 3.2. Level 2.5 functions. Constants of the model are indicated at the top of each plot. They are in the A_1, A_2, B_1, B_2, C_1, C_2, C_3 order. The INF-1 curve indicate values where functions tend to infinity. Here momentum eddy exchange coefficient S_M is plotted.

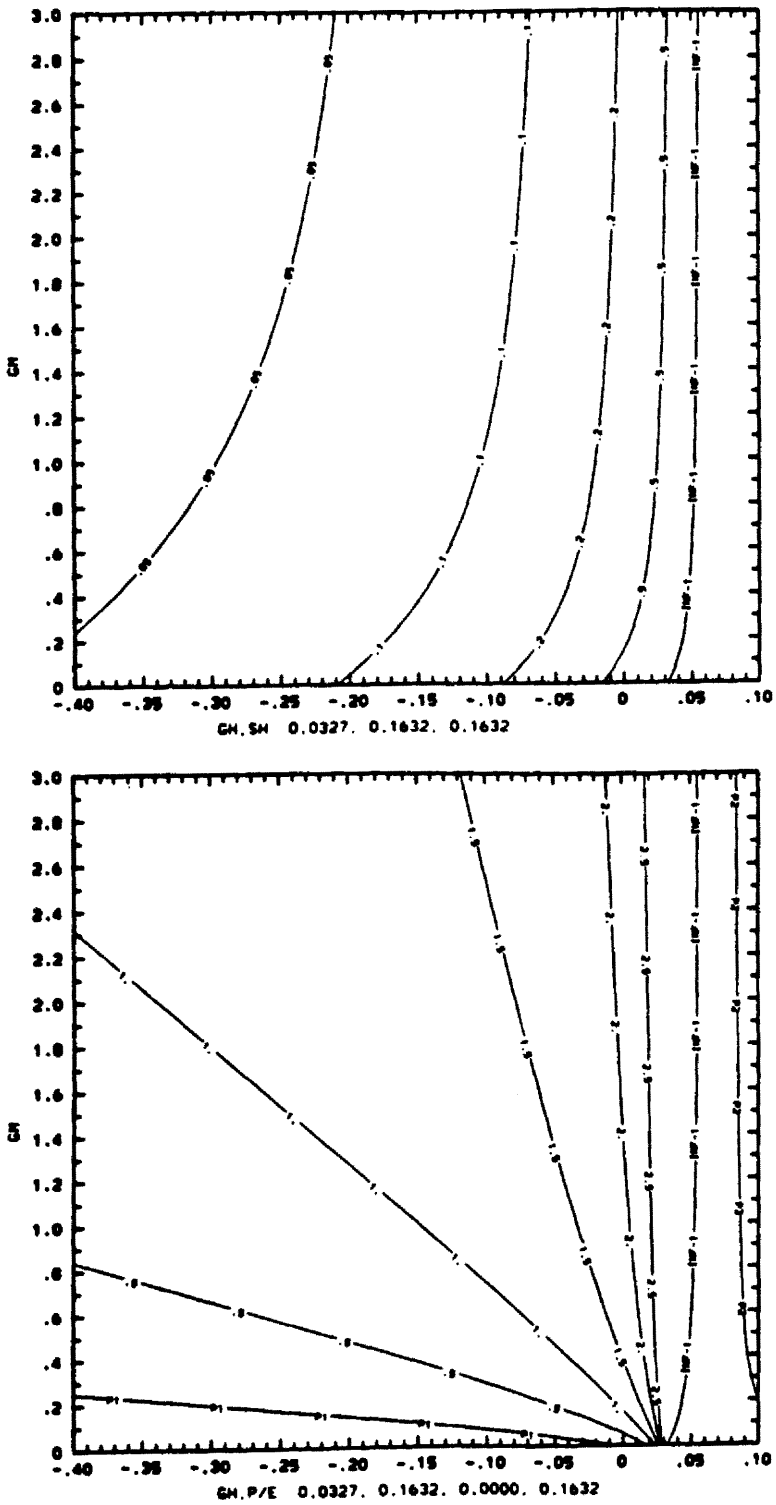

Fig. 3.3. (a) Same as in Fig. 3.2 but for S_H; (b) Same as in Fig. 3.2 but for $(P_s + P_b)/\varepsilon$, P1 curve indicate points where function goes to 0.

Positive definitness of velocity variance lead also to some limits on the possible values of G_H and G_M.

Compare now Figs. 3.2 (S_M) and 3.3b (production/dissipation). Notice also that the gradient Richardson number is given by $Ri = -G_H/G_M$. One can then easily obtain S_M as a function of Ri for constant values of $(P_s + P_b)/\varepsilon$. This way the other results for the Level 2.0 (Fig. 3.1) can be reproduced. Fig. 3.7 combines plots of curves discussed above (i.e., S_M, S_H and $(P_s + P_b)/\varepsilon$) and can be used for tracing S_H, S_M behavior for constant $(P_s + P_b)/\varepsilon$ values. In Fig. 3.7 heavy solid lines are S_M values, S_H values are represented by broken lines, and thin solid lines are $(P_s + P_b)/\varepsilon$ values. For G_M approaching 0 with the constraint $(P_s + P_b)/\varepsilon$ = const. (i.e. traveling down the $(P_s + P_b)/\varepsilon$ isoline), we get a finite value of S_M. This limited value corresponds to infinite (and negative) Richardson number. Notice that $(P_s + P_b)/\varepsilon > 0$ isolines cross the G_H axis for positive, non-zero values of G_H. The above discussion applies to the other turbulent covariances. They all can be expressed as a function of only one mean flow quantity (Richardson number) if a certain constraint on the ratio of the turbulent production to the turbulent dissipation is imposed.

Figs. 3.4-6a,b show turbulent variances of velocity components $\overline{w^2}/q^2$, $\overline{u^2}/q^2$, $\overline{v^2}/q^2$. From eqs 2.18a,b we see that u- and v-variances depend on α. It can be shown that from the point of view of realizability conditions the $\alpha = 0$ and $\alpha = 1$ give the most stringent limitations on the possible G_H values. Therefore, all the results here are presented for $\alpha = 1$ i.e. for $\frac{\partial \bar{V}}{\partial z} = 0$. The $\overline{w^2}/q^2$ is not dependent on α. Examining Fig. 3.4-6 we can see the $\overline{v^2}/q^2$ is positive only for $G_H \leq$

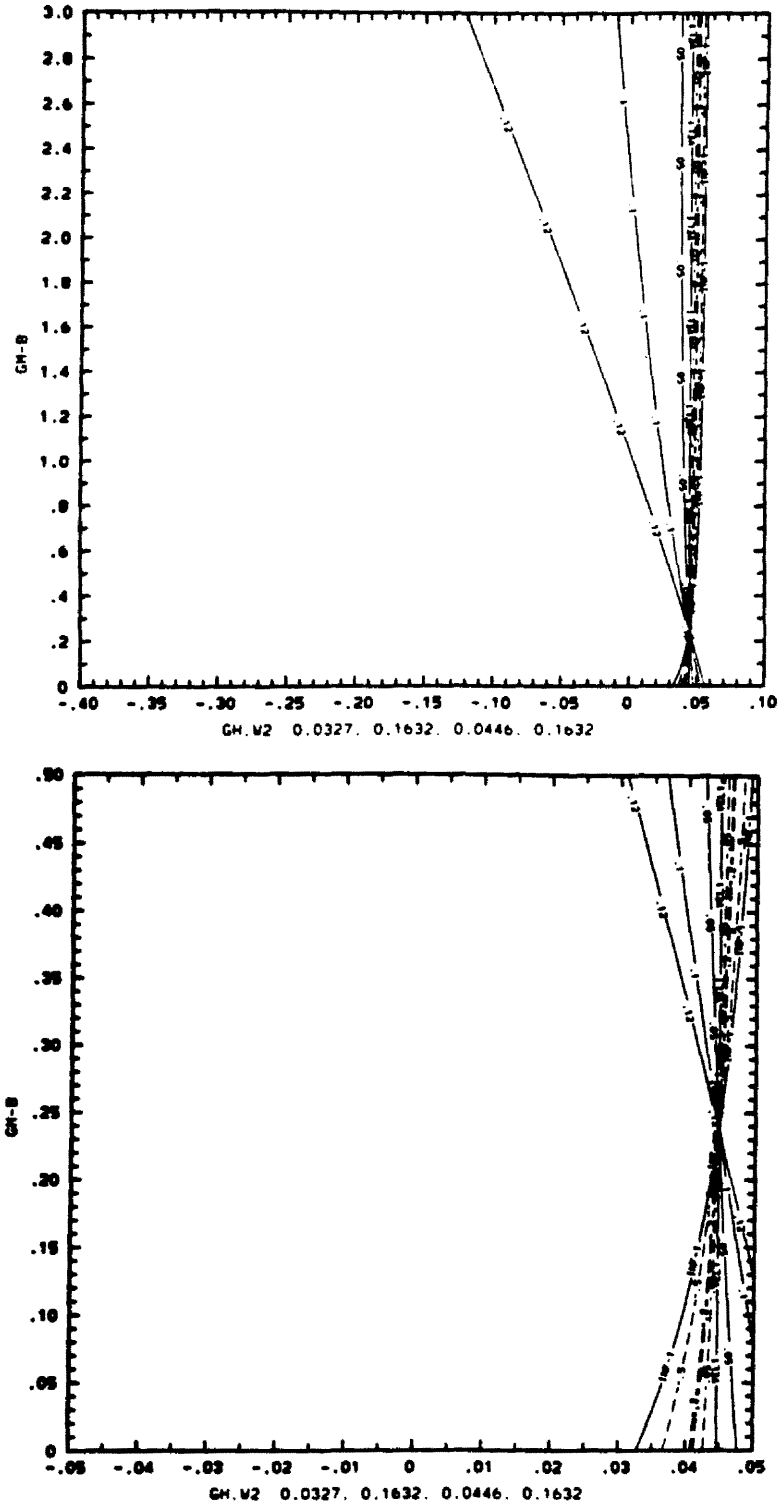

Fig. 3.4. (a) Same as in Fig. 3.2 but for $\overline{w^2}/q^2$ VEL-1 is where function goes to 0, (b) same as (a), different G_H, G_M.

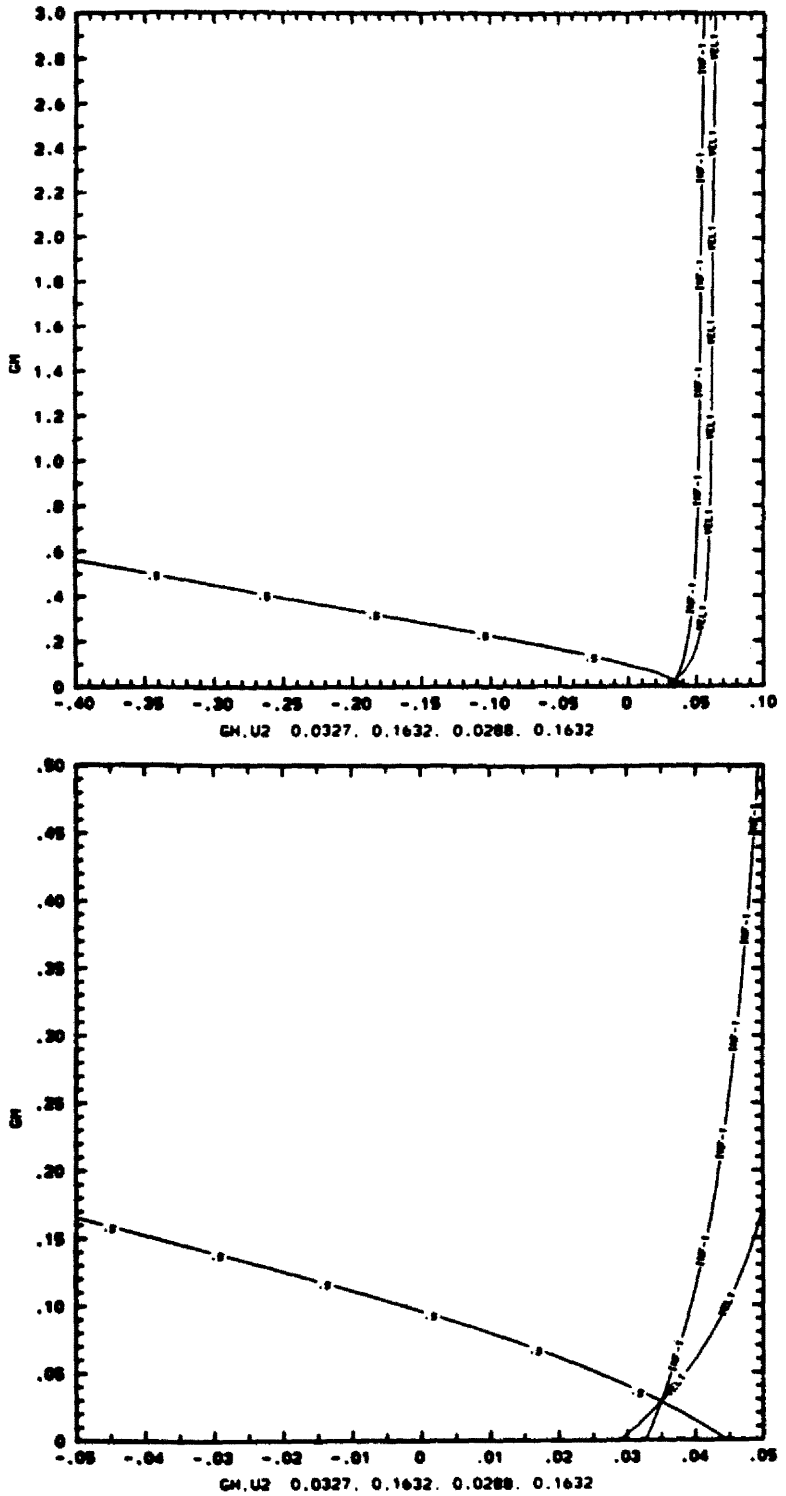

Fig. 3.5. (a) Same as in Fig. 3.2 but for $\overline{u^2}/q^2$ VEL-1 is where function goes to 0, (b) same as (a), different G_H, G_M.

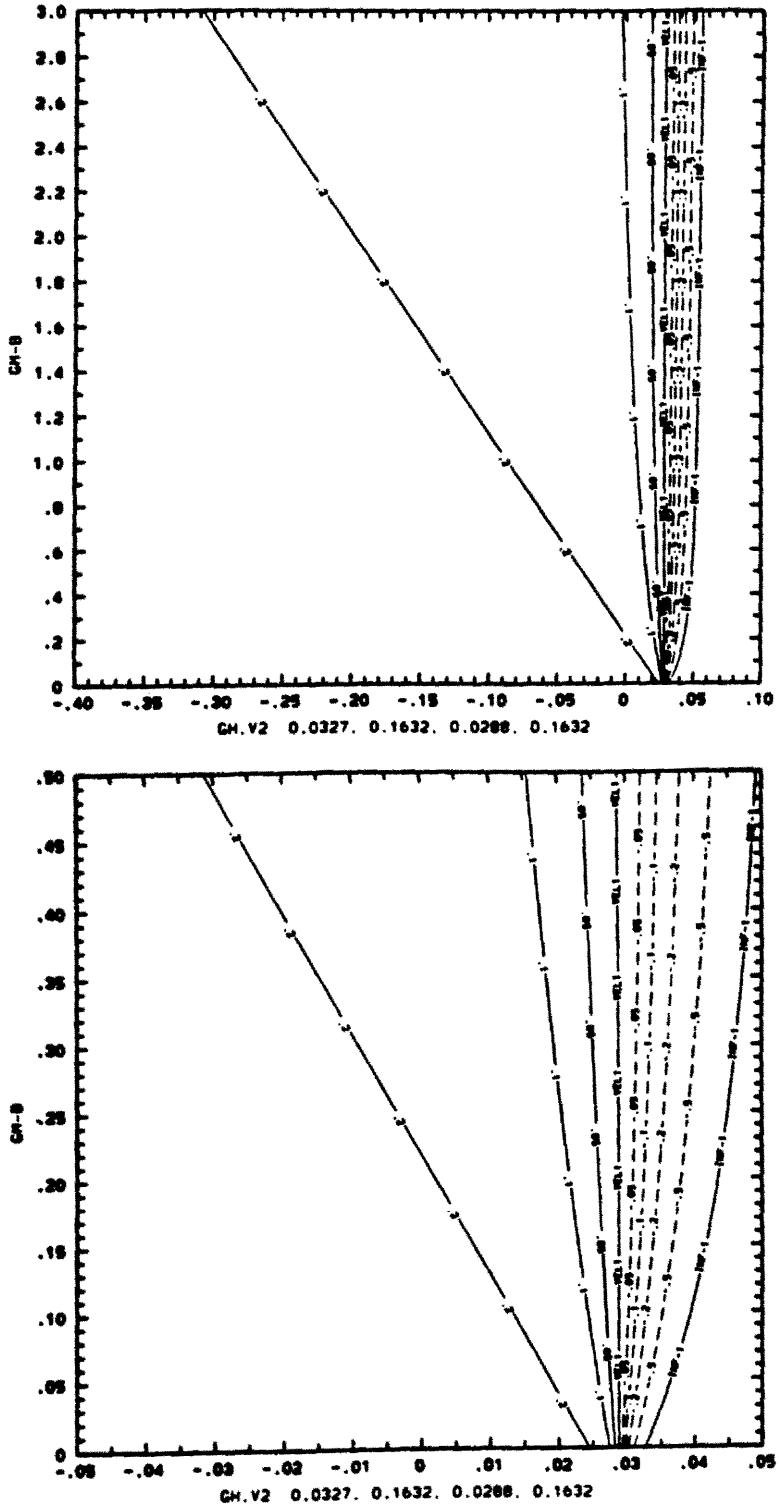

Fig. 3.6. (a) Same as in Fig. 3.2 but for $\overline{v^2}/q^2$ VEL-1 is where function goes to 0, (b) same as (a), different G_H, G_M.

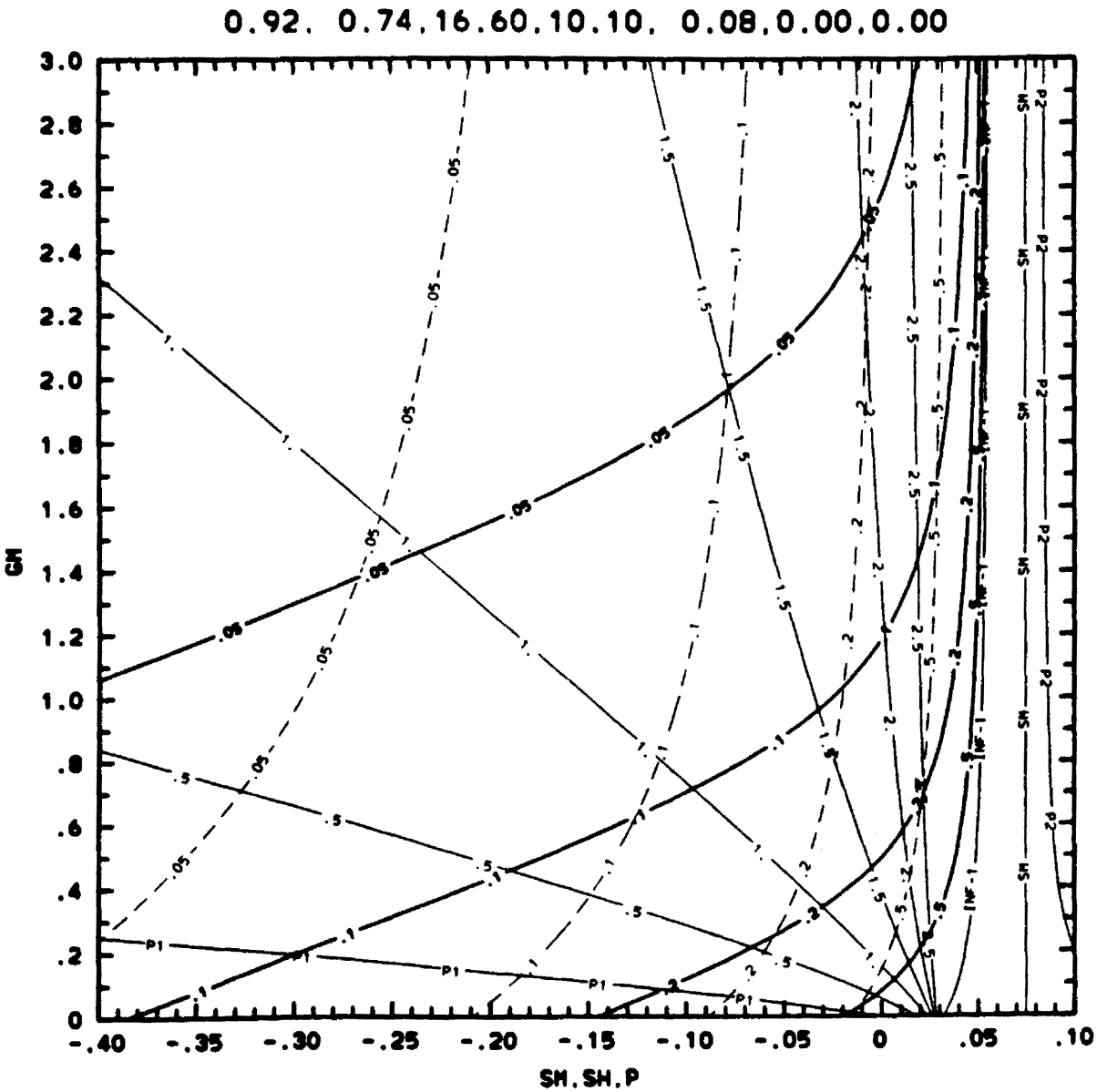

Fig. 3.7. Composite of plots presented in Fig. 3.2 and 3.3. The heavy solid lines indicate S_M functions, broken lines are isolines of S_H and thin solid lines are isolines of the ratio of turbulent production and dissipation. The INF-1 curve gives singular points for all functions. P1 and P2 curves are for $(P_s + P_b)/\varepsilon = 0$.

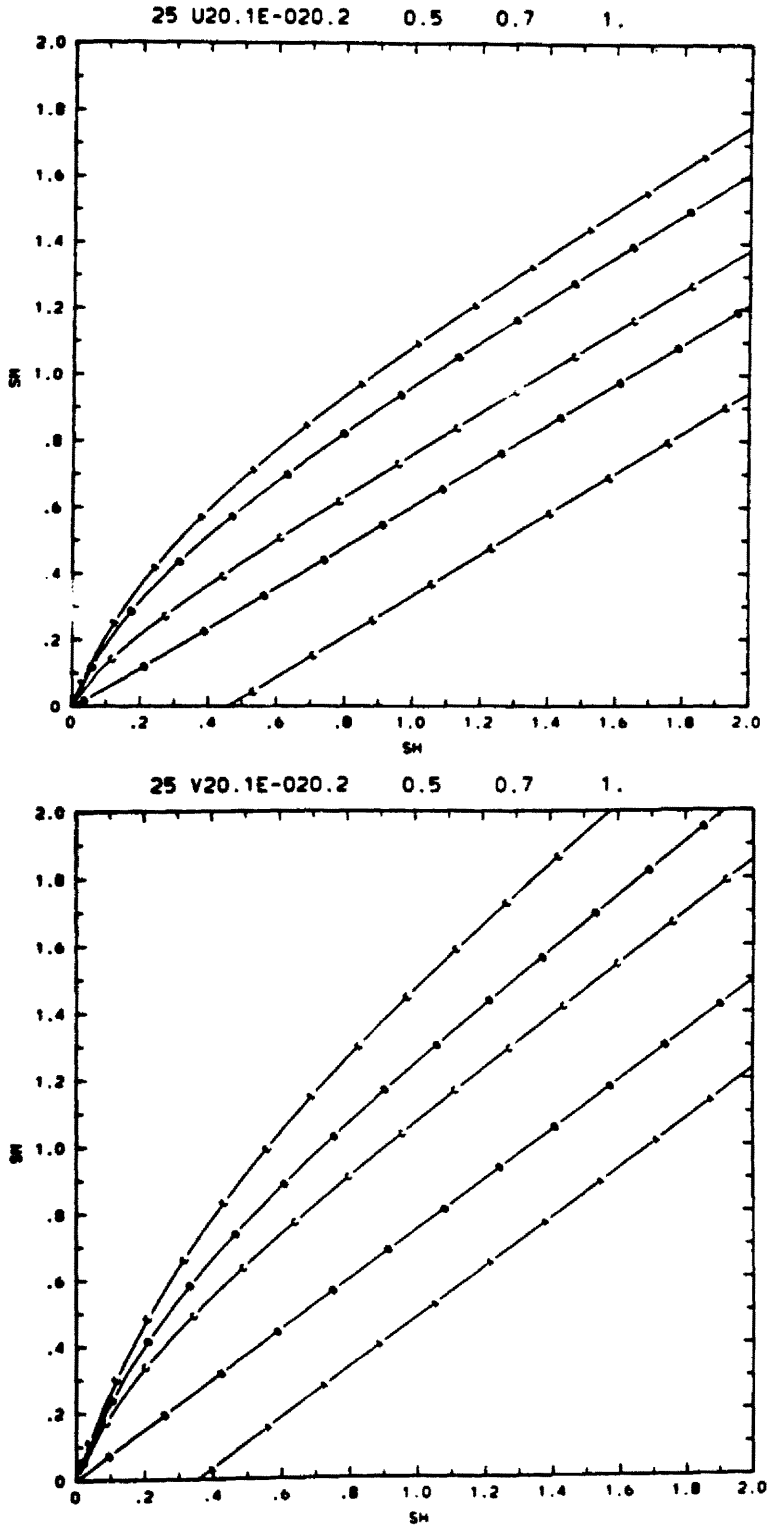

Fig. 3.8. Level 2.5 plots as a function of S_M and S_H. (a) For $\overline{u^2}/q^2$ (b) For $\overline{v^2}/q^2$.

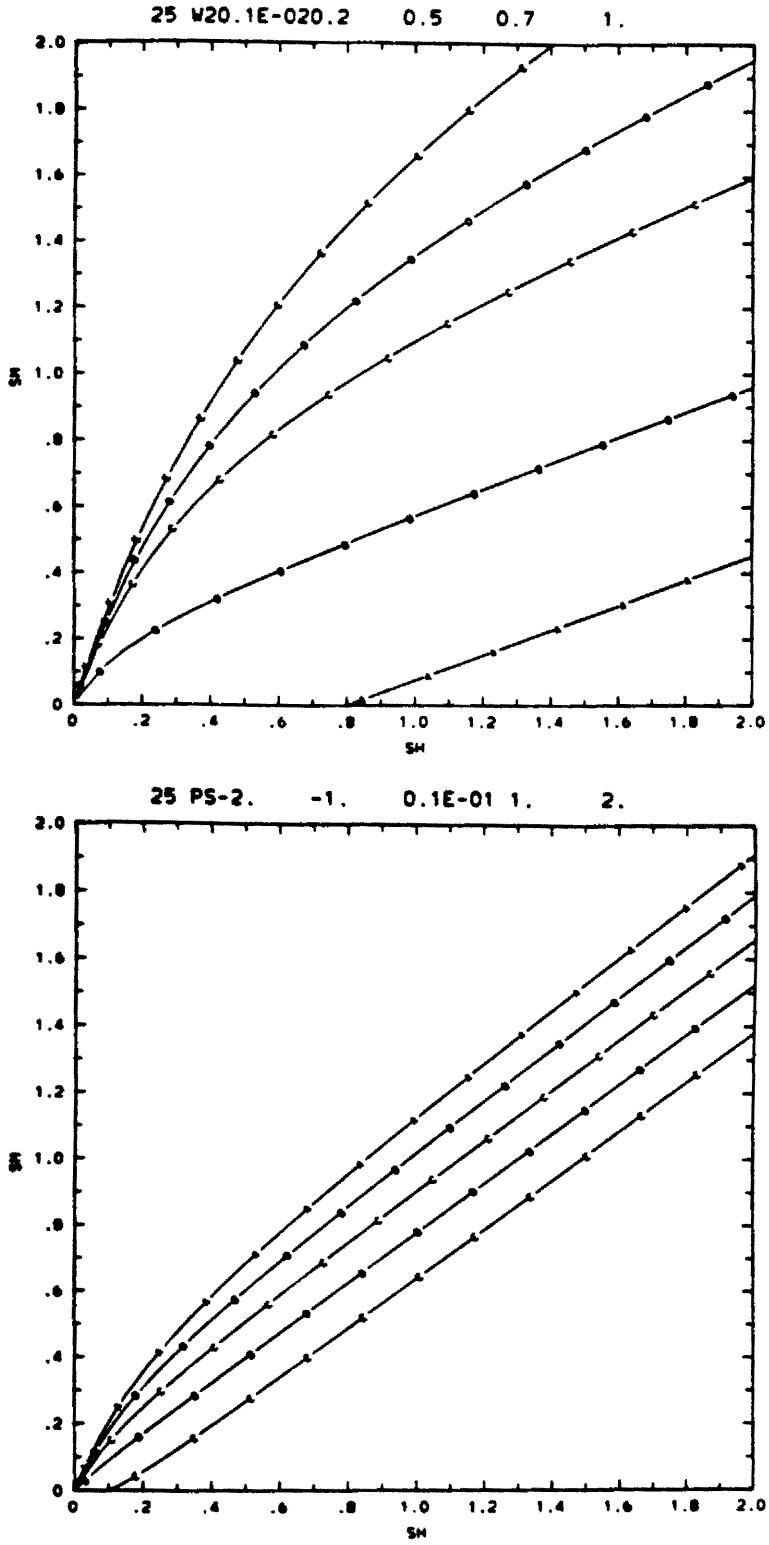

Fig. 3.9. Level 2.5 plots as a function of S_M and S_H (a) $\overline{w^2}/q^2$ (b) $(P_s + P_b)/\varepsilon$.

0.0288, and this limit seems to guarantee positive definiteness of all velocity variances.

Finally we present velocity variances and $(P_s + P_b)/\varepsilon$ as a function of S_M and S_H (Fig. 3.8-9a,b). Again $\alpha = 1$. Only positive and smaller than one isolines are plotted for the velocity variances. The isolines are labelled A,B,C,D, and E and correspond to (0.001, 0.2, 0.5, 0.7, 1.0) values. The isotropic case (all variances equal to 1/3) gives approximately the same values of S_M and S_H. The realizable solution follow this pattern for other velocity variances, i.e. the S_H and S_M values are of the same order.

3.3 Level 3.0

This level of simplification was considerably less investigated and used by researchers. We performed analysis of this model and some of the results are presented in Figs. 3.10-15. Here the additional parameter G_T comes to play making analysis more involved. We plot G_M-G_H dependence of turbulent quantities for 2 different values of G_T = (0.1, 3.0). The range of G_M and G_H is from -6 to 6 on all plots. Values of G_M have to be positive, but negative ones are retained here for illustrative purposes. As before, negative values are plotted as dashed lines. Contours for the normalized (by q^2) velocity variances are chosen at 0.05, 0.2, 0.5 and 1.0 (0.12 instead of 0.2 for the vertical velocity variance). By definition all velocity variances have to be in the (0,1) range. One can see (e.g. in Fig. 3.10) that values (G_M,G_H) giving realizable solutions for the Level 2.5 may now correspond to negative variances. The solutions are highly variable with G_T. The realizable values are, in general, located close to the $(P_s + P_b)/\varepsilon = 1$ isoline.

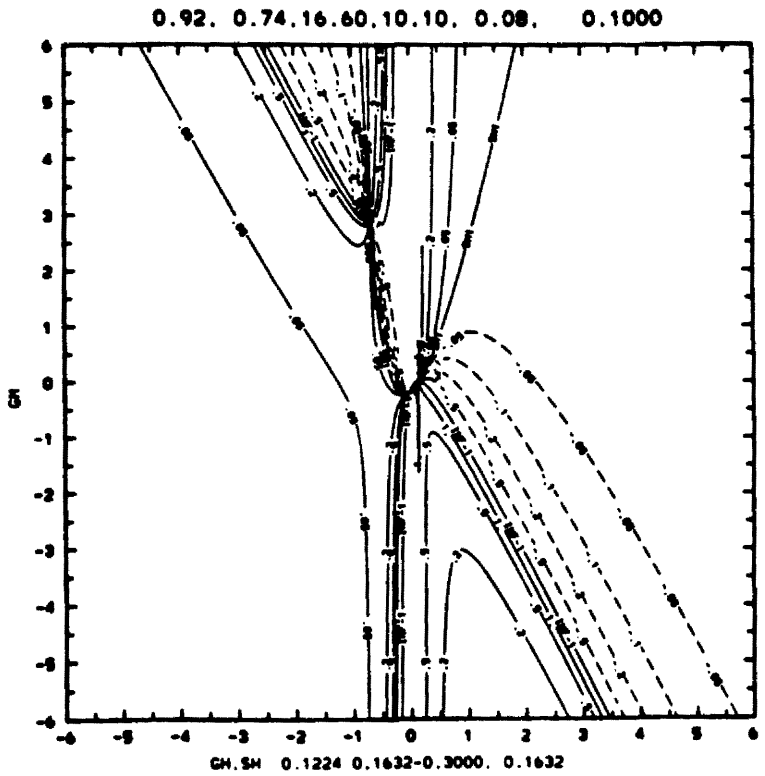

Fig. 3.10. Level 3.0 functions. Constants of the model are indicated at the top of each plot. They are in the A_1, A_2, B_1, B_2, C_1, G_T. The INF-1 curve indicate values where functions tend to infinity. Here $G_T = 0.1$. Numbers at the bottom of each plot indicate G_H values for $G_M = 0$ where the denominator (first two numbers) and numerator (next number or numbers) of the function tend to zero.

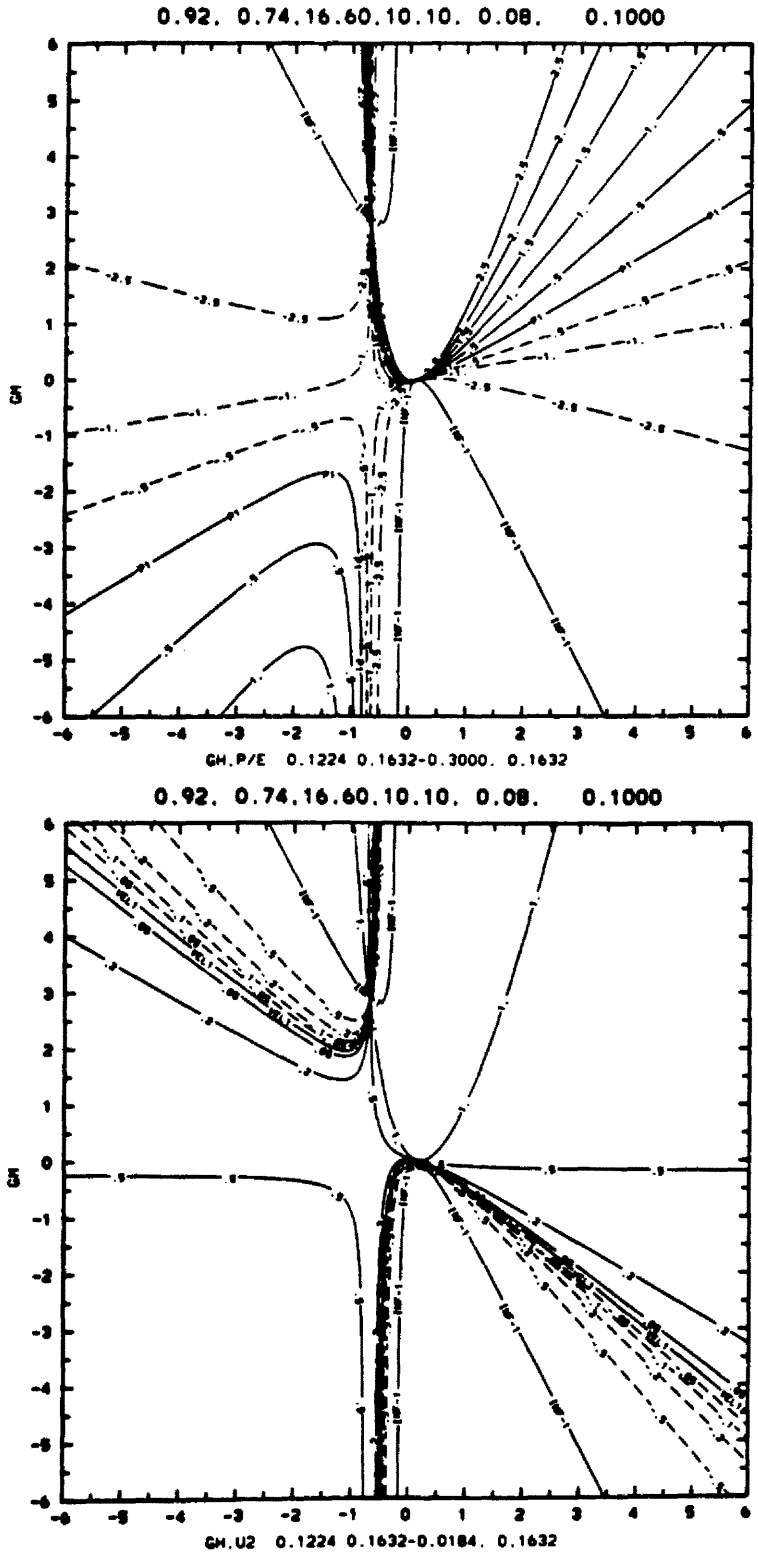

Fig. 3.11. (a) Same as in Fig. 3.10 but for $(P_s + P_b)/\varepsilon$ The P1 curve indicate values of G_M and G_{H_2} where $(P_s + P_b)/\varepsilon$ goes to zero. (b) Same as (a) but for $\overline{u^2}/q^2$.

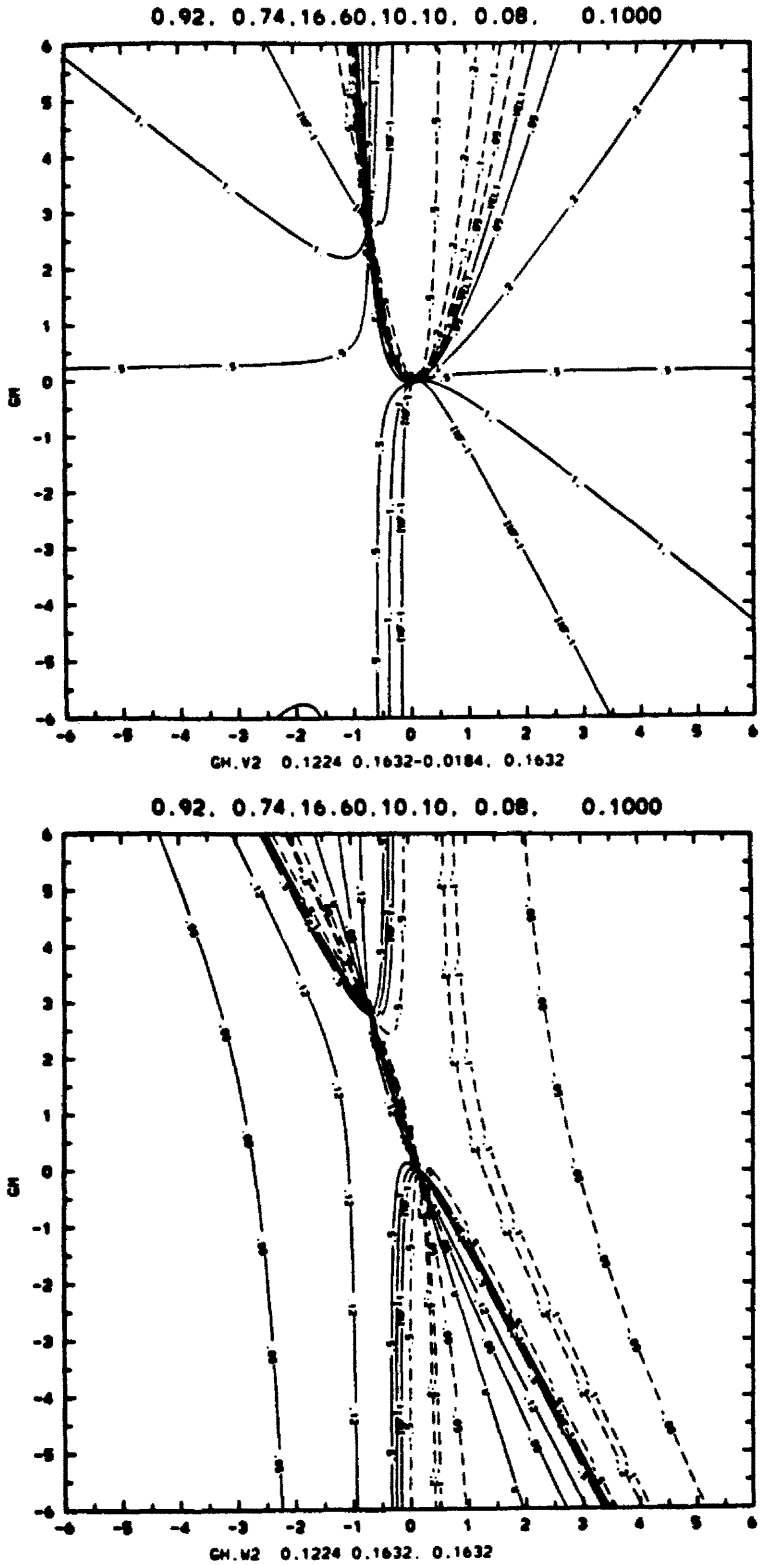

Fig. 3.12. (a) Same as in Fig. 3.10 but for $\overline{v^2}/q^2$ (b) Same as in Fig 3.10 but for $\overline{w^2}/q^2$.

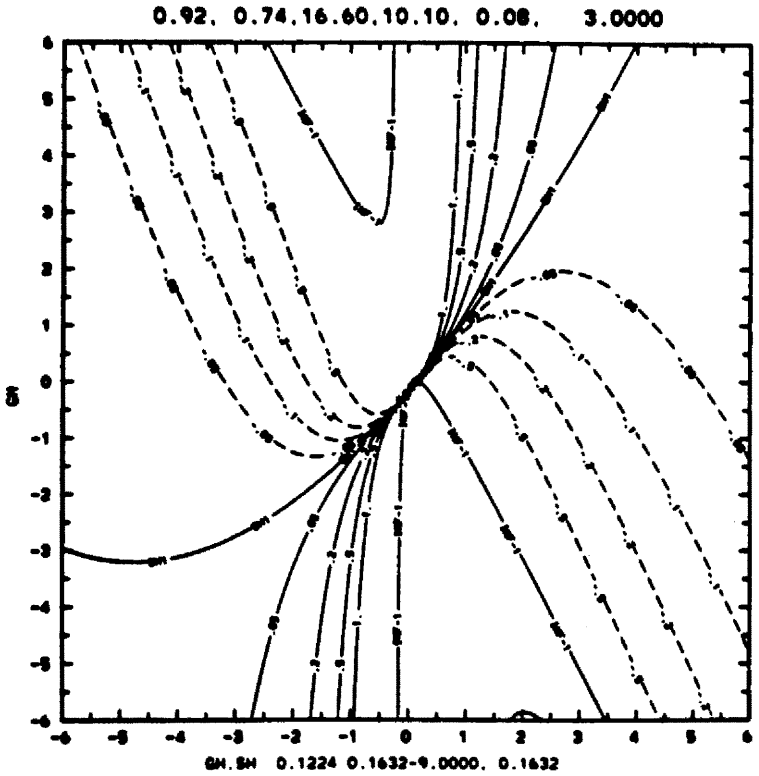

Fig. 3.13. Same as in Fig. 3.10 but for G_T = 3.0.

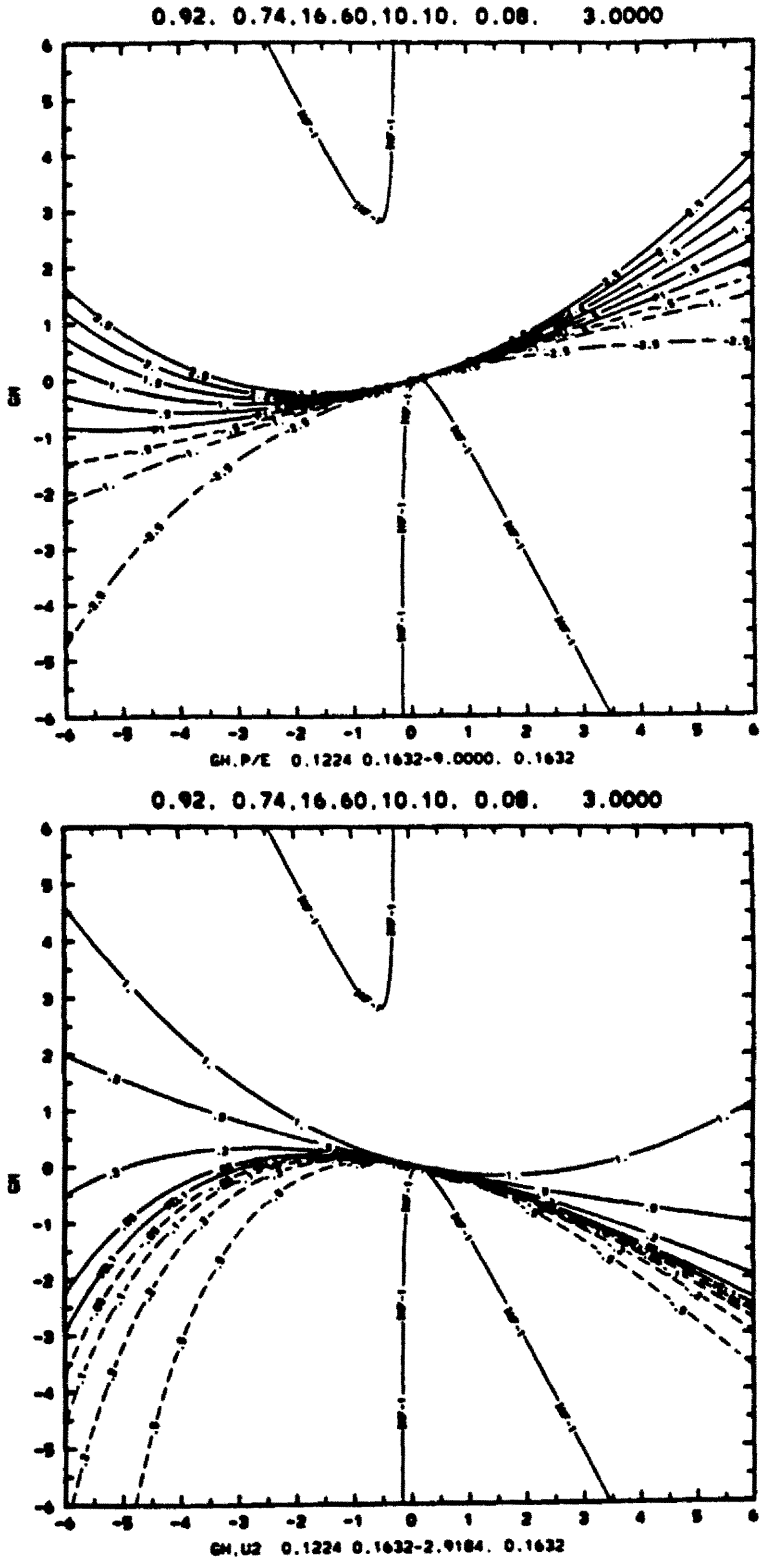

Fig. 3.14. Same as in Fig. 3.11 but for G_T = 3.0.

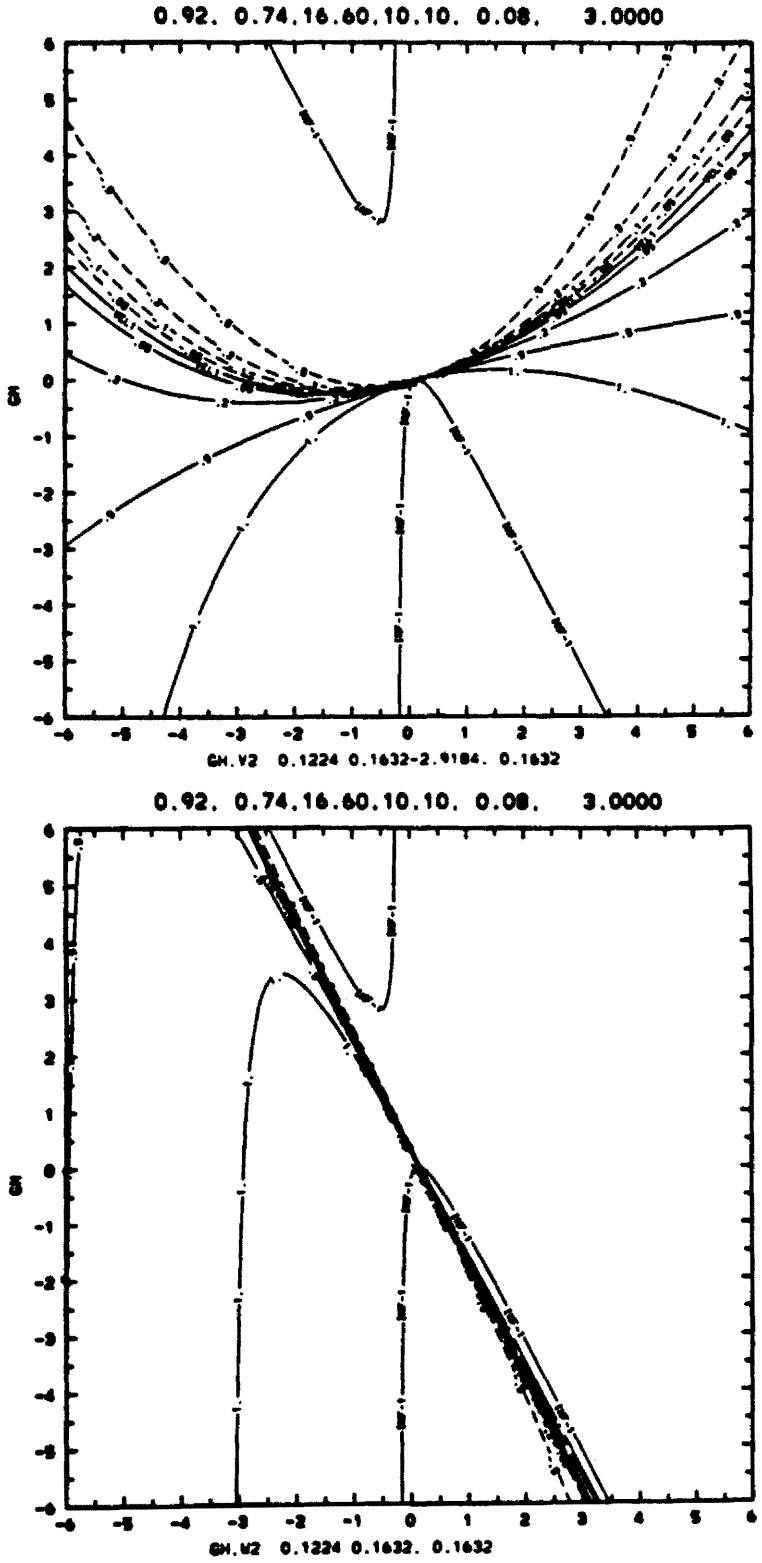

Fig. 3.15. Same as in Fig. 3.12 but for G_T = 3.0.

We diagnostically calculated Level 3.0 functions from the numerical results of our runs of the Level 2.5 model. The results indicated that the Level 3.0 produces very stringent conditions on the G_M and G_H values. The picture is still not clear: however, we hope to obtain some diagnostic results from the working Level 3.0 model (Burk, personal communication).

3.4 Comments on realizability conditions

Mellor and Yamada mention negative variances, e.g., in their 1982 and 1974 papers, and discuss realizability conditions in connection with some model problems (MY, 1982). In the 1974 paper they state that: "The components $\overline{u^2}$, $\overline{v^2}$ and $\overline{w^2}$ should, of course, be positive definite. This turns out to be true in practice everywhere in the Level 2 calculation and nearly so for Levels 3 and 4 where, however, small negative values appeared between 0700-0800 (after a discontinuity in the tendency of wall temperature) at a couple grid points." In their 1982 paper they state that "...we have had occasional difficulty with the level 2 1/2 model; for some model simulations a discontinuity in velocity could develop and persist." Hassid and Galperin (1983) and Helfand and Labraga (1985) also discuss some realizability conditions they had to impose.

It seems that the model does not properly handle transitory phenomena but has the ability to adjust the mean flow and turbulence to consistently physical values. As long as variances are not used explicitly (for example to diagnose triple correlation terms) but are just diagnosed, the fact that they are negative is only annoying. The slowly varying phenomena, e.g., dry boundary layer on a sunny day - as in the Wangara case - are predicted well by the low order second-order

closure. The apparent failure of level 3.0 and 2.5 to predict highly variable flows can probably be traced down to the basic assumption of Mellor and Yamada -- namely scaling out the advection and diffusion terms in almost all equations. At the top of the stratocumulus layer where intensive, local (radiative) cooling is distributed mainly through turbulent diffusion and where gradients of stratification are strong, the assumption of the small role of diffusional terms can be a weak one. It is true, though, that the model is driven towards the local equilibrium. Imagine vigorous TKE advected to otherwise undisturbed region. Parameterization of dissipation provides negative feedback in the TKE equation

$$\frac{\partial q^2}{\partial t} = \ldots - \frac{q^3}{\Lambda_2},$$

and the model will adjust to local equilibrium. This fact is probably the only justification of usage of the level 2 model together with a prognostic equation for the TKE (this scheme was used by Yamada, 1983 and is implemented in RAMS). Such a scheme, by definition, cannot take into account situations which are strongly out of equilibrium. The other comment here is the way to approach non-realizable solutions. One way (M-Y, 1982) is to change <u>mean flow</u> values and wait for turbulence to adjust to a new mean flow so it produces physically consistent turbulent quantities. The other way is to apply the clipping approximation, that is to keep everything which should be positive to some small but positive (may be zero) value. The idea behind this approach is similar: change <u>turbulence</u> so it will adjust to the mean flow, and the mean flow will contribute to realizable turbulence.

4. EDDY EXCHANGE COEFFICIENTS - EXPERIMENTAL AND NUMERICAL RESULTS

In this chapter we compare eddy exchange coefficients as deduced from Chen and Cotton's full second-order closure model (Level 3.5) with Level 2.0 and with some experimental results. We try to provide here transition between analytical studies (Chapter 2 and 3) and a numerical one (Chapter 5). We indicate the possible limitations of the simplified turbulence models.

4.1 Experimental Results on Eddy Exchange Coefficients

In the seventies, many observations of the ABLs (Atmospheric Boundary Layers) were carried out, especially in the surface layer. The surface layer measurements (e.g. Businger et al., 1971) give a consistent picture, and the use of the Monin-Obukhov theory facilitates data interpretation. On the other hand, measurements in the outer layer (above the surface layer) are more troublesome. One problem results from the difficulty of having the full set of measuring equipment placed in the outer layer (especially in the marine boundary layer). The second problem results from the difficulties in measurements of mean gradients (which are small in unstable case) and turbulent fluxes (for a stable stratified atmosphere). Our discussion here will be based on papers by Ueda et al. (1981) and Weber et al. (1975). These measurements were performed from the meteorological towers in the outer PBL.

Weber et al. (1975) carried out wind measurements at six levels on the TV tower (18.3, 91.4, 137.2, 182.9, 243.8, 304.8). These measurements were taken at the Savannah River Laboratory Facility during

a sixteen-day period between 13 May and 29 May, 1973. Climet cup and bivane systems were mounted in each of the six levels. Slow response aspirated temperature sensors were located at 3.0, 36.6, 91.4, 137.2, 182.8, 335.3 meters. Additional fast response instruments were attached to two booms mounted at 18.3 meters. The data were time-averaged over a 40-minute period. One of many turbulent statistics presented in the Weber paper is the ratio of eddy diffusivities K_H/K_M. These are presented in figures 4.1 and 4.2. The turbulent Prandtl number exhibits large scatter for the near neutral conditions. On the stable side the ratios are larger than on the unstable side and approach a value between 1 and 2 for large stability parameter z/L.

The paper by Ueda, et al. (1981) compares laboratory, tower and theoretical predictions for K_H, K_M and their ratio. The micrometeorological observations were carried out by the Meteorological Research Institute during the period July 26 to August 1, 1977. To obtain the momentum and heat fluxes, fluctuating wind components were measured with five three-component sonic anemometers mounted at altitudes of 25, 50, 100, 150 and 200 meters on the 213 m tower. Temperature fluctuations at the same elevations were obtained with thermocouples. Additional surface measurements were performed at location 1.5 m above the ground. A kitoon was used to obtain the gradients of the wind speed, temperature and humidity. The averaging period was 10 minutes. The results are presented in Fig. 4.3. The normalization functions are

$$K_{M0} = ku_*z$$

and

$$K_{H0} = 1.2K_{M0}.$$

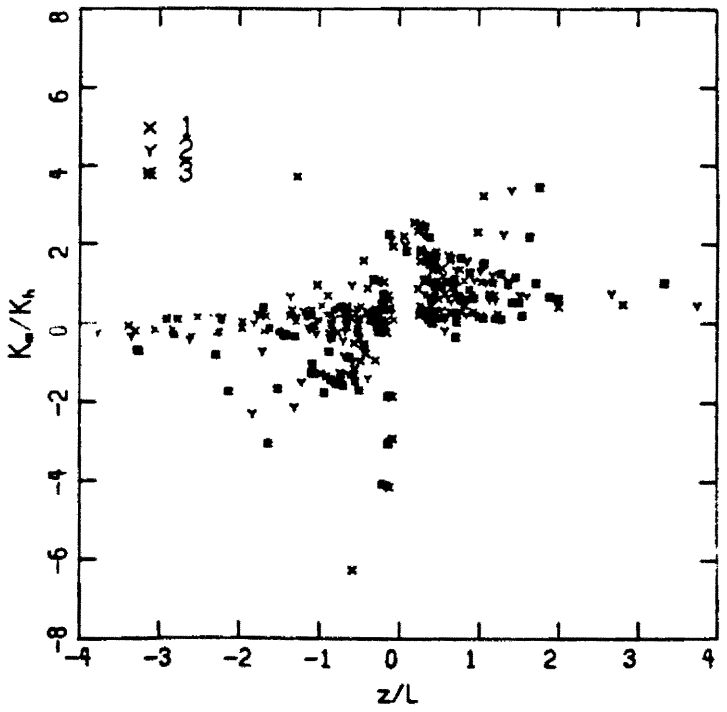

Fig. 4.1. Ratio of momentum and heat diffusivity versus z/L. Symbols correspond to measurement heights of 91 m (1) and 137 m (2) without L.W. and S.W. radiation. [From Weber et al.].

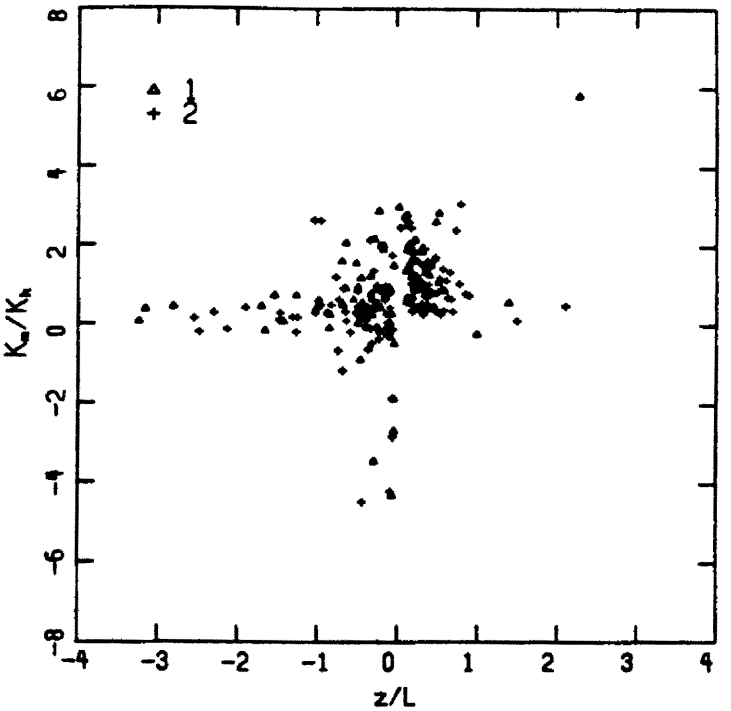

Fig. 4.2. Ratio of momentum and heat diffusivity versus z/L. Symbols correspond to measurement heights of 183 m (1), 244 m (2), and 305 m (3). [From Weber et al., (1975)].

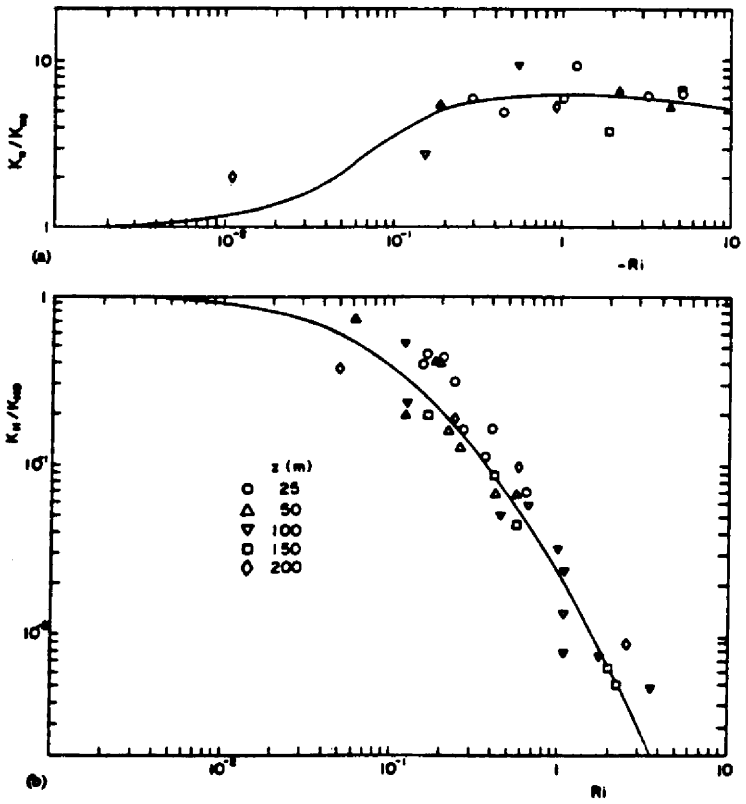

Fig. 4.3. Variation of the ratio K_H/K_{Ho} with stability in the lower atmosphere, compared with that observed in the laboratory experiment. Solid lines represent the empirical fit. [From Ueda et al., (1981)].

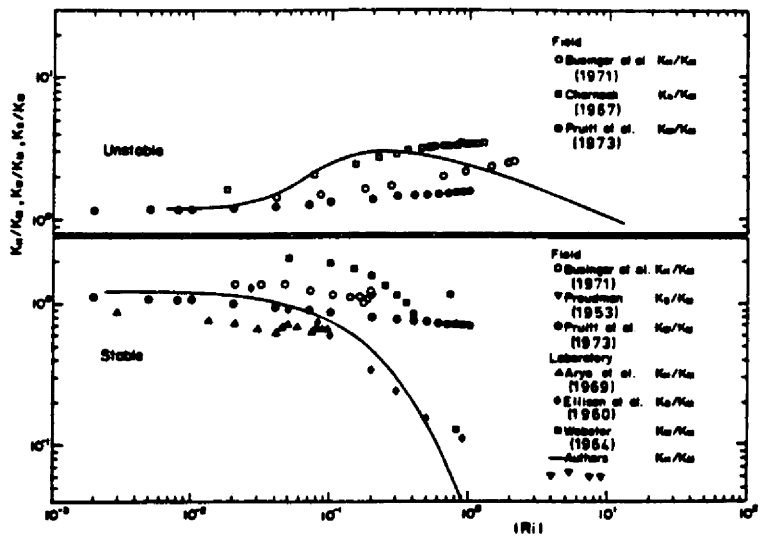

Fig. 4.4. Comparison of the Ueda's et al., (1981) (line labeled Authors) results on K_H/K_M with those of other investigators. [From Ueda et al., (1981)].

The authors mention that under extremely stable conditions an upward heat flux occurs against the temperature gradient. This results in a negative value of the eddy diffusivity; these results are omitted. Under stable conditions the ratio K_H/K_{H0} decreases rapidly as the Richardson number increases and attains a value of 0.01 at Ri about 1.6. On the other hand, in unstably stratified flows the K_H/K_{H0} increases with -Ri, but for -Ri > 0.2 which is normally encountered in the atmosphere, it retains a constant value of 6.0. The continuous line in the same diagram represents the laboratory results (Komori, et al.,1982). However, according to authors, the field observation results published up to 1981 do not show a trend similar to that in their work. The authors conclude that the difference (especially for the stable layer) is probably due to the different level of the atmosphere observed, i.e., in the outer versus surface layer. The K_H/K_M behaviour is presented in Fig. 4.4. Again, for stable conditions Ueda's results show a much larger dependence of the K_H/K_M ratio on the stratification rather than on other (surface layer) measurements. For unstable conditions, previous observations in the surface layer show an increase of the ratios K_H/K_{H0} and K_H/K_M with increasing -Ri under weakly unstable conditions. This is consistent with Ueda's results. Under strongly unstable conditions, the ratio K_H/K_M decreases with -Ri, approaching the value of $K_H/K_M = 1$ at Ri about -10.0. This last result is different from that in the surface layer where the ratio K_H/K_M continues to increase with increasing instability.

We will now briefly summarize the above findings:

1. The surface layer results are not always consistent with the results obtained in the outer layer (Ueda).

2. The countergradient (negative K_H and K_M) are observed for regions near strong inversions (Ueda) and for the near neutral flow (Weber).
3. The scatter of data is considerable for the near neutral flow (Weber).
4. For the stable region, K_H and K_H/K_M decrease remarkably with the gradient Richardson number (Ueda).
5. For the unstable conditions, K_H/K_M remains constant or decreases slightly (Ueda).

4.2 Eddy Exchange Coefficients Derived from Chen and Cotton's Model. Comparison with Level 2.

In this paragraph we discuss eddy exchange coefficients obtained from the Chen and Cotton model. Figs 4.5-9 present results for the simulation of Wangara Day 33 case, and Fig 4.10 shows results for the stratocumulus case. We actually re-run both cases with the higher vertical resolution in hope that apparent randomness will decrease, but otherwise the model is the same as that described in Chen and Cotton (1983a,b) and Chen (1984). From the gradients of mean quantities and corresponding fluxes we were able to derive eddy exchange coefficients. The local Richardson number was calculated, and the results are presented in the form of a scattergram. On the same figures, plots (solid lines) of Level 2 functions are given. Slightly modified ZL constants are used. We summarize the findings as follows:

1. Eddy exchange coefficients, as prognosed by the level 3.5 model, can be negative. This indicates countergradient fluxes. The Level 2.0 model always predicts positive values of S_M and S_H.
2. In the stable regime (for flux Richardson number greater than critical Richardson number) turbulence exists and is non-vanishing

in the Level 3.5 model. It is evident in all figures. The Level 2.0 predicts the critical Richardson value above which the turbulence do not exist.

3. In the unstable regime the order of magnitude of S_H and S_M is comparable with the Level 2 model. Still, the comparison is not perfect and the differences are considerable.
4. Theory predicts that S_M for u-component and v-component of velocity vector is the same. From the figures (Fig 4.5 and 4.7) presented here, one can see that this is only approximately true. The scalar quantities S_H and S_q (Fig 4.6 and 4.8), where q is the total water, are clearly not equivalent, and the scatter of values is considerable.
5. Although it can not be seen from the figures presented here, further analysis shows that the prediction of eddy exchange coefficients vary with height and with the time periods considered. For the initial time of model evolution, the adjustment time, the Level 3.5 model S_H, and S_M functions deviate more from the theory. On the other hand, one may picture initial model development as corresponding to the transition periods in nature. We sometimes filtered values above the inversion (plots with INV CUT label). In this stable region, calculation of eddy exchange coefficients is uncertain because mixing there is small and the fluxes do not adjust to the mean gradients.

We will try now to summarize experimental (previous paragraph), numerical (Chen and Cotton, Level 3.5 model), and analytical (Level 2) findings. Both experimental and Level 3.5 model results indicate existence of countergradient fluxes. The numerical model may

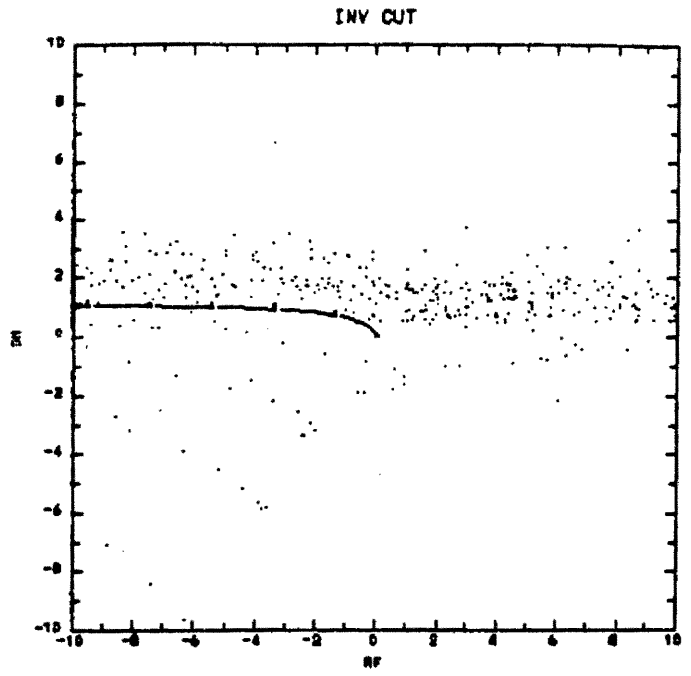

Fig. 4.5. Non-dimensional momentum exchange coefficient for u-component of velocity as a function of flux Richardson number R_f. Dots represent results from analysis of the level 3.5 closure model; solid line is obtained from level 2 model. Level 3.5 data do not contain points above the inversion layer (data filtered).

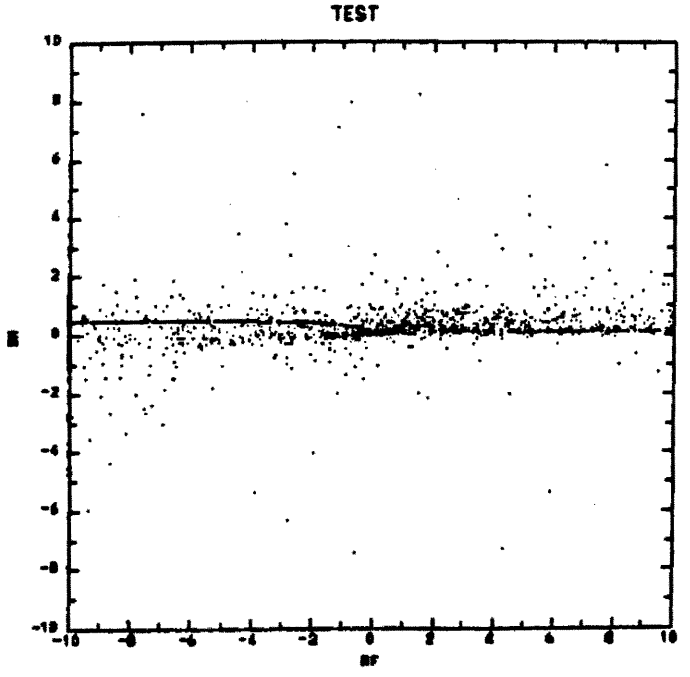

Fig. 4.6. Same as Fig. 5, but for heat eddy coefficient S_H.

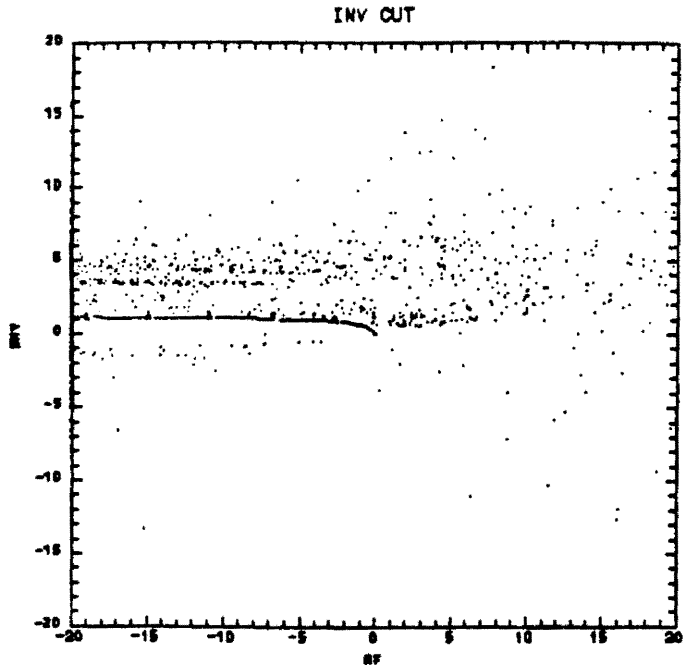

Fig. 4.7. Same as Fig. 5, but for v-component of velocity (data filtered).

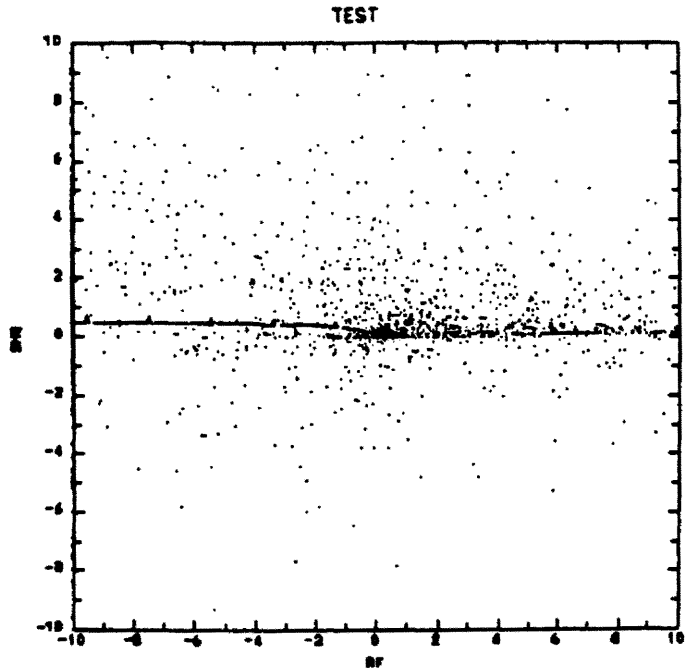

Fig. 4.8. Same as Fig. 5, but for total water.

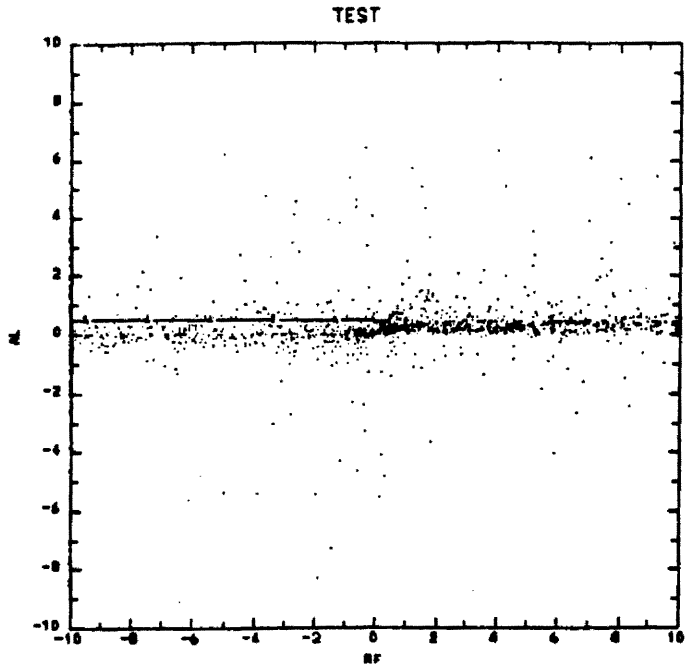

Fig. 4.9. Same as Fig. 5, but for turbulent Prandtl number.

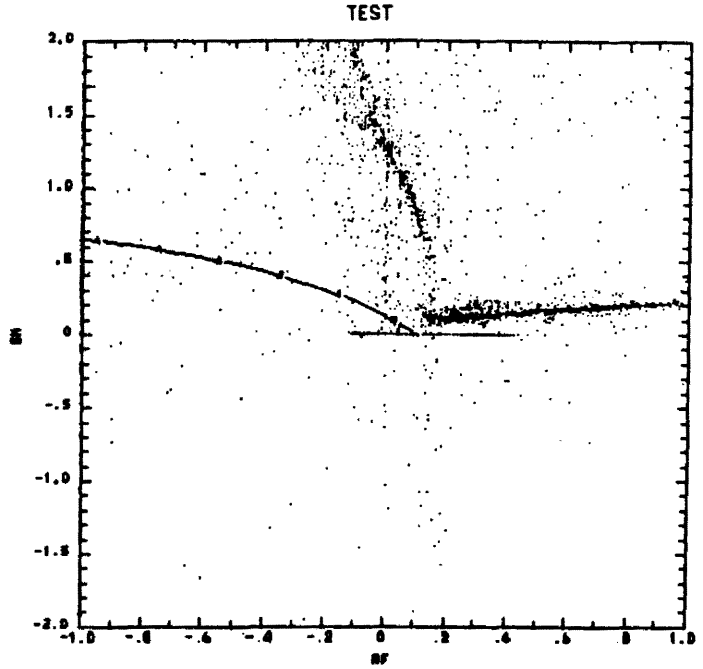

Fig. 4.10. Same as Fig. 5, but for stratocumulus case.

additionally introduce its own numerical 'negative physics' due to, for example, coarse resolution in the top of the entrainment layer. On the other hand, the Chen and Cotton model has a mechanism for the countergradient transport--the ZL parameterization of triple-correlation diffusional terms. The Level 2.0 model fails here. It means that the (a) local equilibrium assumption, (b) neglecting diffusional terms, (c) too simple third order closure - contribute to model failure. One should interpret what is being said here as an indication of Level 2.0 model limitations; not a demonstration of the superiority of the Level 3.5 model.

Both experiment and the CC model show that turbulence exists above the critical Richardson number. Level 2.0 predicts a critical Richardson number (although it is defined by Yamada (1975) as the largest value of Ri for which model is still realizable). Considerable scatter exists in both experimental and in CC model results. We think that some of the scatter in the CC model is purely numerical (see point 5 above). Some of the scatter in the experiment can be related to measurement error, but it can be the result of the technique of data presentation. Simply put, the data do not uniquely scale with one parameter (in our case either z/L or Ri) above the surface layer. From the CC model results and comparison with the Level 2.0 model, one may deduce that any approach based on diagnostic S_H, S_M should be undertaken with some caution.

5. NUMERICAL SIMULATION - CALIFORNIA STRATUS CASE

In this chapter we discuss results of numerical simulations of stratocumulus case described by Brost et al. (1982a,b). We concentrate on results obtained from the Level 2.5 model but occasionaly compare it with the Level 4 (full second-order closure) model. At the end we discuss in more general terms applicability of the second-order closure theory.

5.1 Stratocumulus Cloud

In this paragraph we present results obtained from the numerical integration of homogeneous Atmospheric Boundary Layer (ABL) topped by stratocumulus layer. The case is similar to that described by Brost et al. (1982a,b) and Albrecht et al. (1985), and was investigated in detail by Chen (1984). Here we try to see if it is feasible to study the stratocumulus with the simplified second-order closure model. The numerical model is that described in detail in Chapters 2 and 3. In addition, we developed a Level 4 model with twenty-one prognostic equations. We make some comparison of these models. The model was integrated on the grid consisting of 41 points with the vertical resolution of 25 meters; the last points were stretched up to two kilometers to allow proper functioning of the radiation scheme. The staggered grid is used with all variances and co-variances at the w-points. The surface heat and moisture fluxes are based on the Louis (1979) drag coefficient formulation (numerical fit to the Businger et al. (1971) profiles). The variances and co-variances are diagnosed at

the surface from the Manton and Cotton (1977) parameterization. The Manton and Cotton model is based on the Mellor and Yamada Level 2 scheme with empirical input based on Bussinger et al. (1971) surface layer profiles. The results compare well with the empirical one (see, for example, Panofsky and Dutton, 1984, pp 160-173). The radiation scheme and the sub-grid condensation scheme are activated (see description in Chapter 2). The realizability conditions for the Level 2.5 are imposed (see Chapter 3).

The initial conditions are those for the solid cloud case off the coast of California for 1315-1319 GMT 17 June 1976 described by Albrecht et al. (1985). The model was integrated for two hours. The initial turbulent kinetic energy (TKE) profile was constant and equal to 0.15 m^2 s^{-2}. Figs. 5.1a,b show time series of the surface momentum flux u_*^2 and of w^2 . The vertical velocity variance (Fig. 5.1b) time series is plotted for six levels. These are at the grid point 2 (curve labelled A), 5 (curve B), 10 (curve C) , 20 (curve D), 30 (curve E), and 41 (curve F). Initially w-variance at the lower layers (curves A and B) exhibits rapid growth up to 0.9 m^2 s^{-2}. But after approximately ten minutes of simulation time, it begins to decrease and then stabilizes after one hour. Above the inversion layer (approx. 550 meters) w-variance rapidly decreases to zero--compare curves E and F. The u_*^2 momentum flux takes on values close to 0.25 m^2 / s^2 after one hour of model run. We estimate the model's adjustment time to be on the order of one hour. The subsequent results are for 5400s and 7200s of model simulation. The initial length scale was taken from the work of Enger (1983) and is essentially a global prescription based on stability and the height of planetary boundary layer (PBL). This length scale is

applied only for 200 seconds and replaced by the locally diagnosed length scale as described in Chen and Cotton (1983a,b). We feel that the length scale definition is particularly important for the lower levels of a second order closure model because of its essential role in the modeling of the dissipation and production terms. The dissipation term ε is inversly proportional to l, and production and buoyancy terms are proportional to dissipation $P_b = \varepsilon B_1 S_H G_H$, and $P_s = \varepsilon B_1 S_M G_M$. The fluxes, which are proportional to l, tend to zero for small l, no matter how large the TKE. The advection of fresh and vigorous TKE may result in its total dissipation with no net effect. It seems that most modelers apply some more or less random schemes, having in mind the particular application. The final justification is a comparison of model results with experiment or with more sophisticated models. This approach is taken here. In Figs. 5.1c,d plots of U and V component of mean velocity are shown. We set U and V values to zero at the bottom for all integration time. There is a large wind gradient at the top of the boundary layer. Brost et al. (1982a,b) conclude that the structure of the boundary layer in the case being considered depends strongly on the shear generated turbulence production at the top of the PBL. The other term is, according to Brost et al., the infrared cooling. We can see in Fig. 5.1f that the potential temperature profile is indeed destabilized by the IR cooling. Fig. 5.2b presents the turbulent kinetic energy. There is a small secondary maximum close to the top of PBL. The heat flux profile (Fig. 5.2c) exhibits negative values just below the cloud top related to the entrainment of dry and warm air from above the inversion. In Figs. 5.3a,b,c the total water, cloud water,

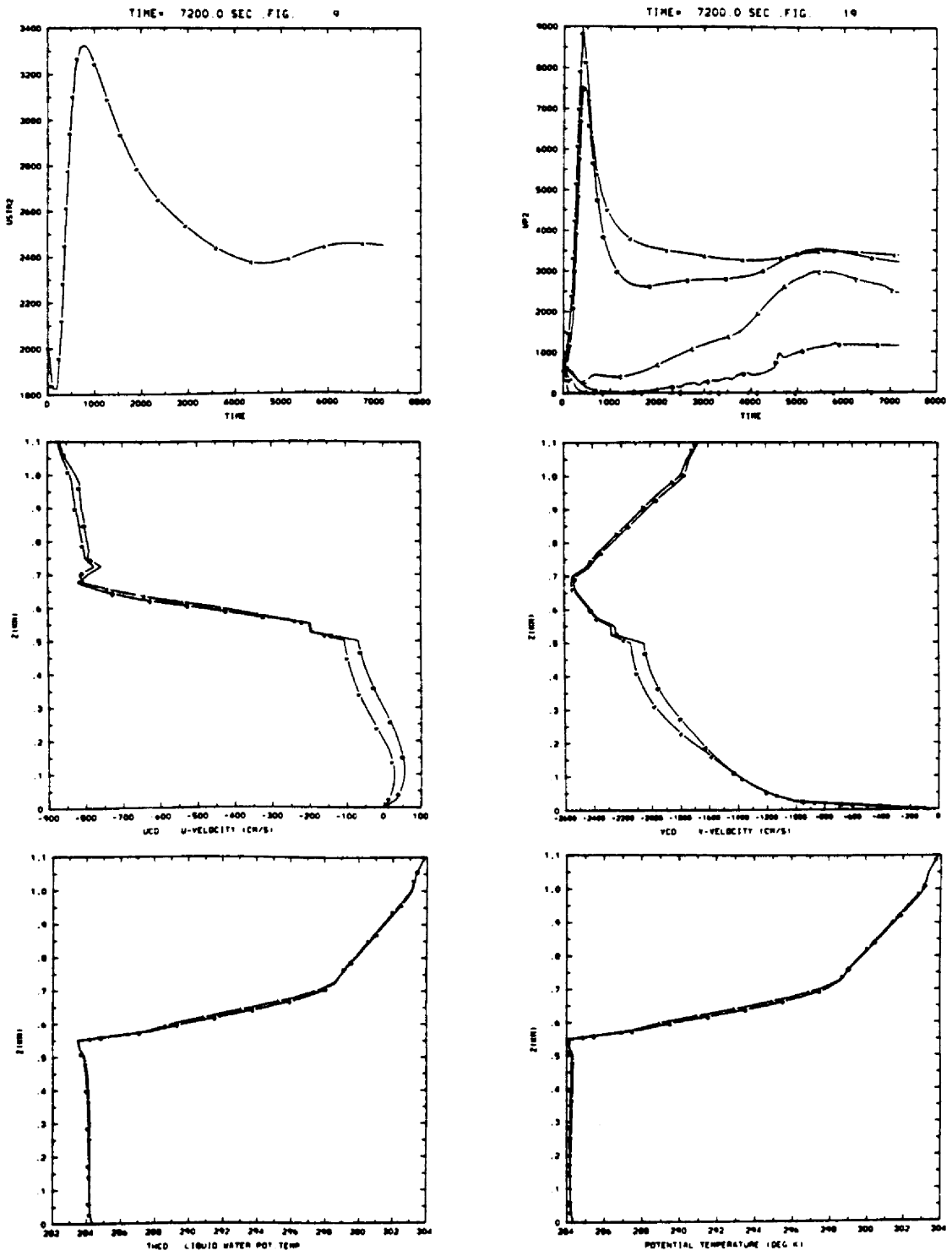

Fig. 5.1. (a) Time series of surface momentum flux, (b) Time series of w-variance, Vertical profiles of (c) U, (d) V, (e) θ_{il}, and (f) θ.

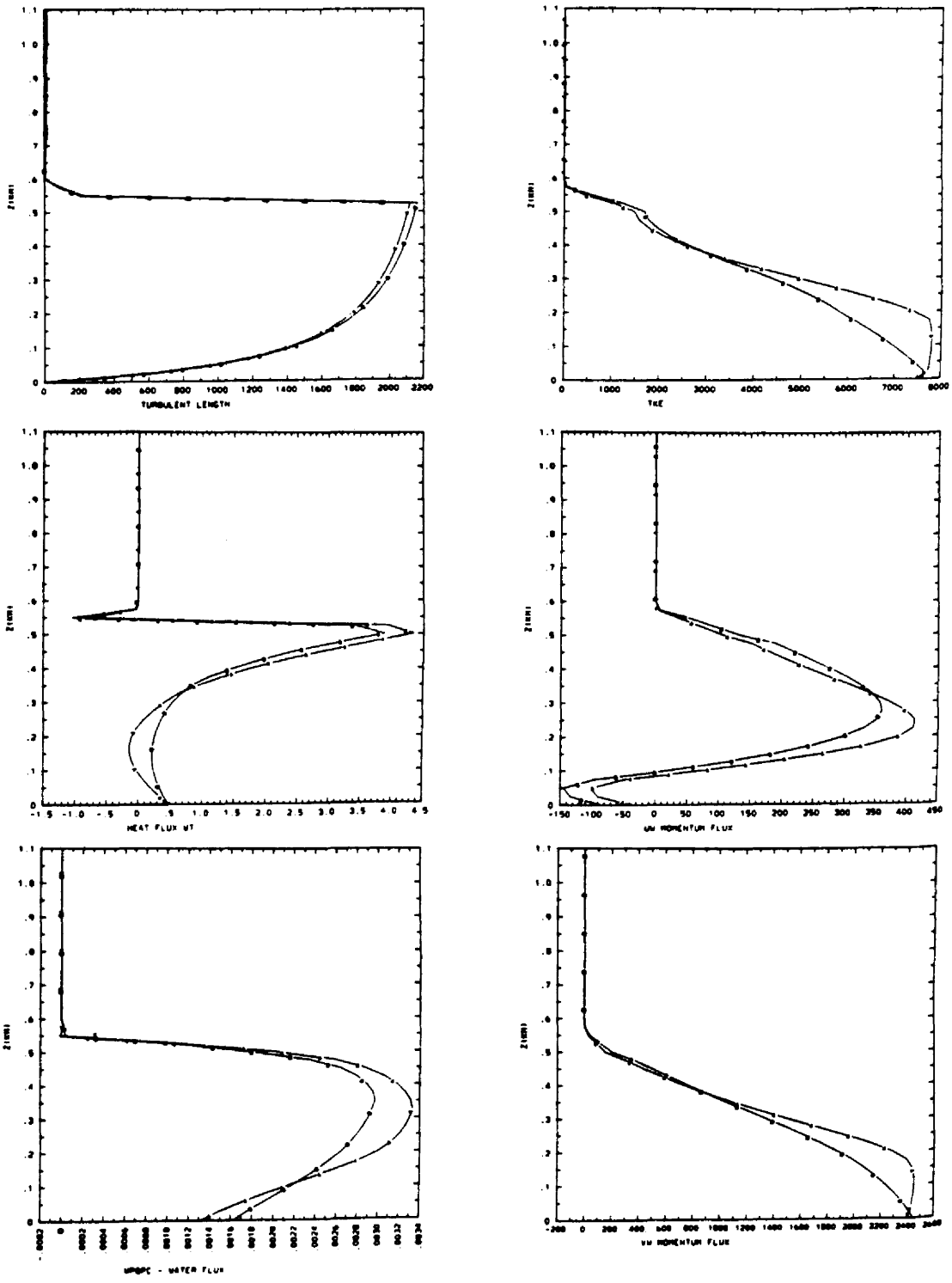

Fig. 5.2. Vertical profiles of (a) Turbulent length, (b) Turbulent kinetic energy, (c) Vertical heat flux, (d) uw-momentum, (e) Water flux, and (f) vw-momentum.

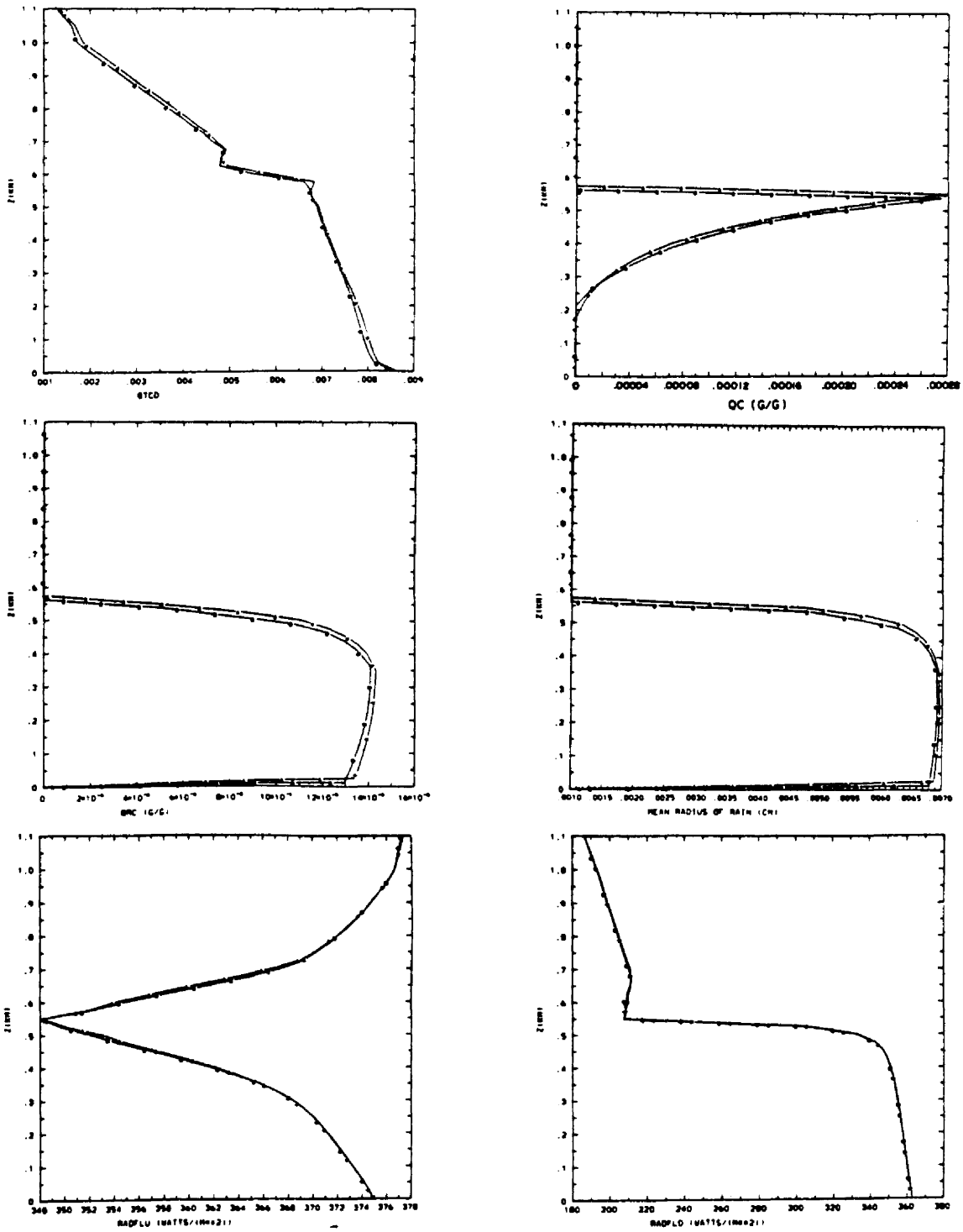

Fig. 5.3. Vertical profiles of (a) Total water, (b) Cloud water, (c) Rain water, (d) Mean radius of rain, (e) Upward radiation flux, and (f) Downward radiation flux.

and rain water mixing ratios are presented. The radiative profiles are shown in Figs. 5.3e,f. The radiative divergence is well concentrated (approximately 50 meters below the inversion). The maximum of cloud water near the top of PBL and the dryness of the overlying air mass are responsible for this radiation profile. Two height-time profiles are presented in Figs. 5.4-5. The negative heat flux builds in gradually at the top of cloud layer. In the next 3 figures (Figs. 5.6-8a,b) we compare result obtained from Level 2.5 and Level 4 models. The time plots for the Level 2.5 model are for 200s, 900s, 1800s, 5400s, and 7200s of the model simulation time (upper figure). They are the same for the Level 4.0 (lower figure) except that 200s are replaced by 0s. Again, the initial profiles for both models should be interpreted cautiously. For example, curve C for the Level 4.0 is at 0.5 h of simulation time, well within model adjustment time. The magnitude of the negative heat flux at the top of the boundary layer and the TKE profile are similiar for both models. The potential temperature profile seems to be more unstable in the 2.5 Level case. The agreement between the models seems to be good.

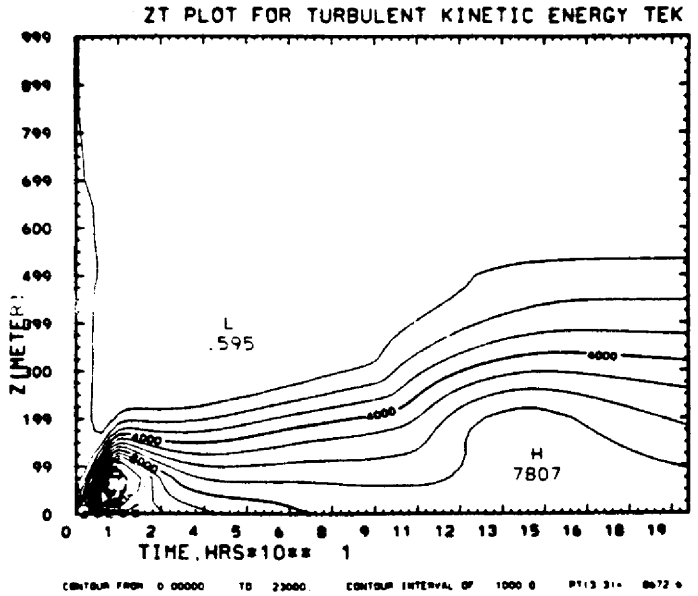

Fig. 5.4. Time-height cross-section of turbulence kinetic energy.

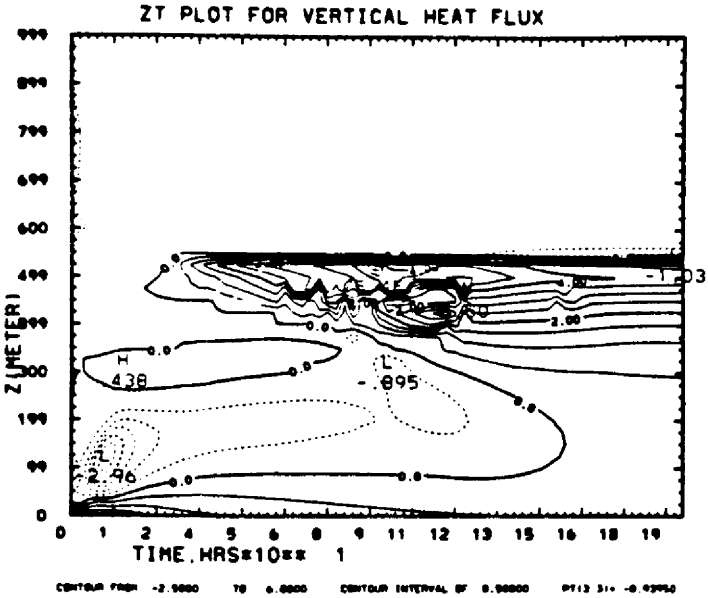

Fig. 5.5. Time-height cross-section of vertical heat flux.

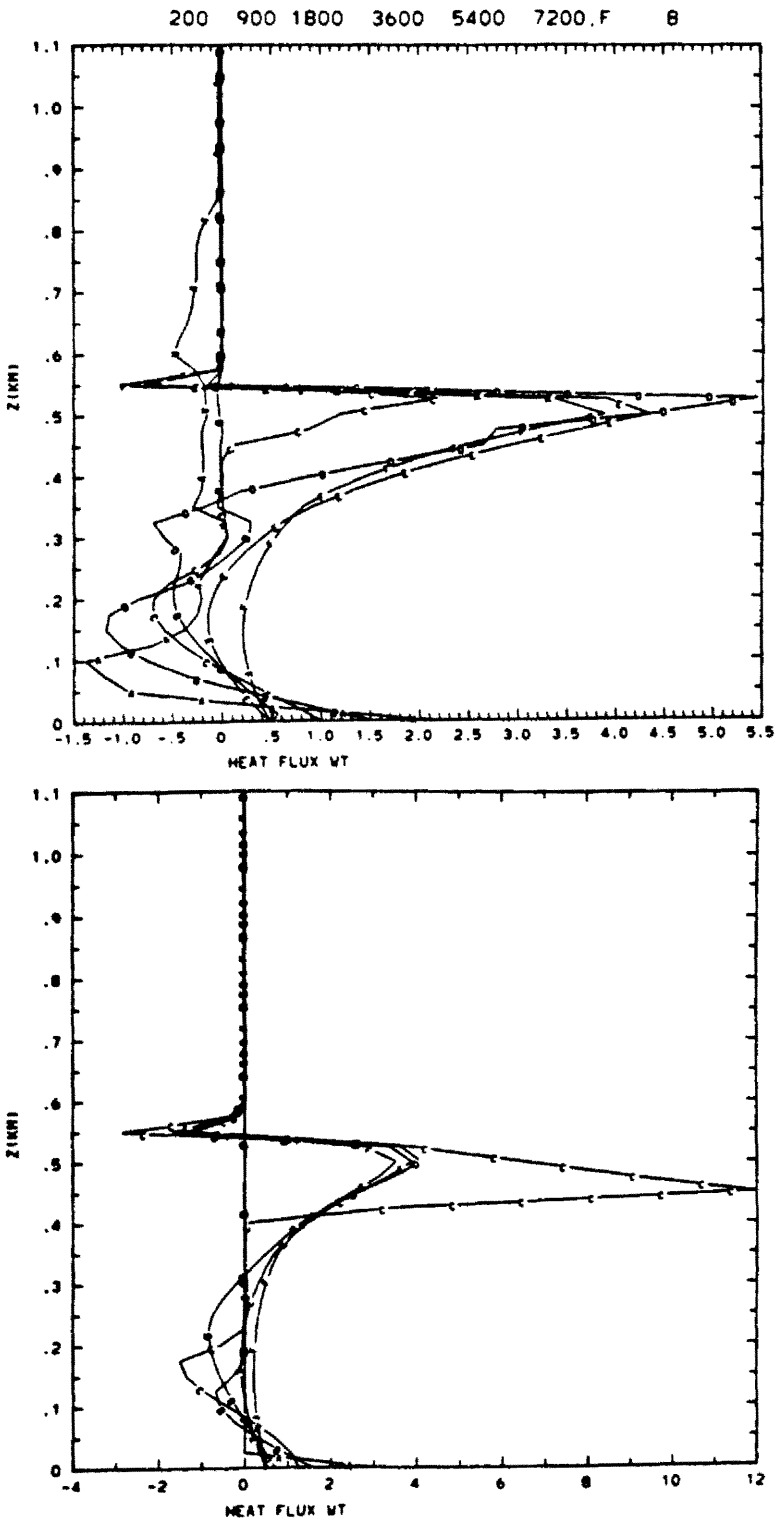

Fig. 5.6. Comparison of heat vertical heat flux as predicted by (a) Level 2.5 model and (b) Level 4.0 model.

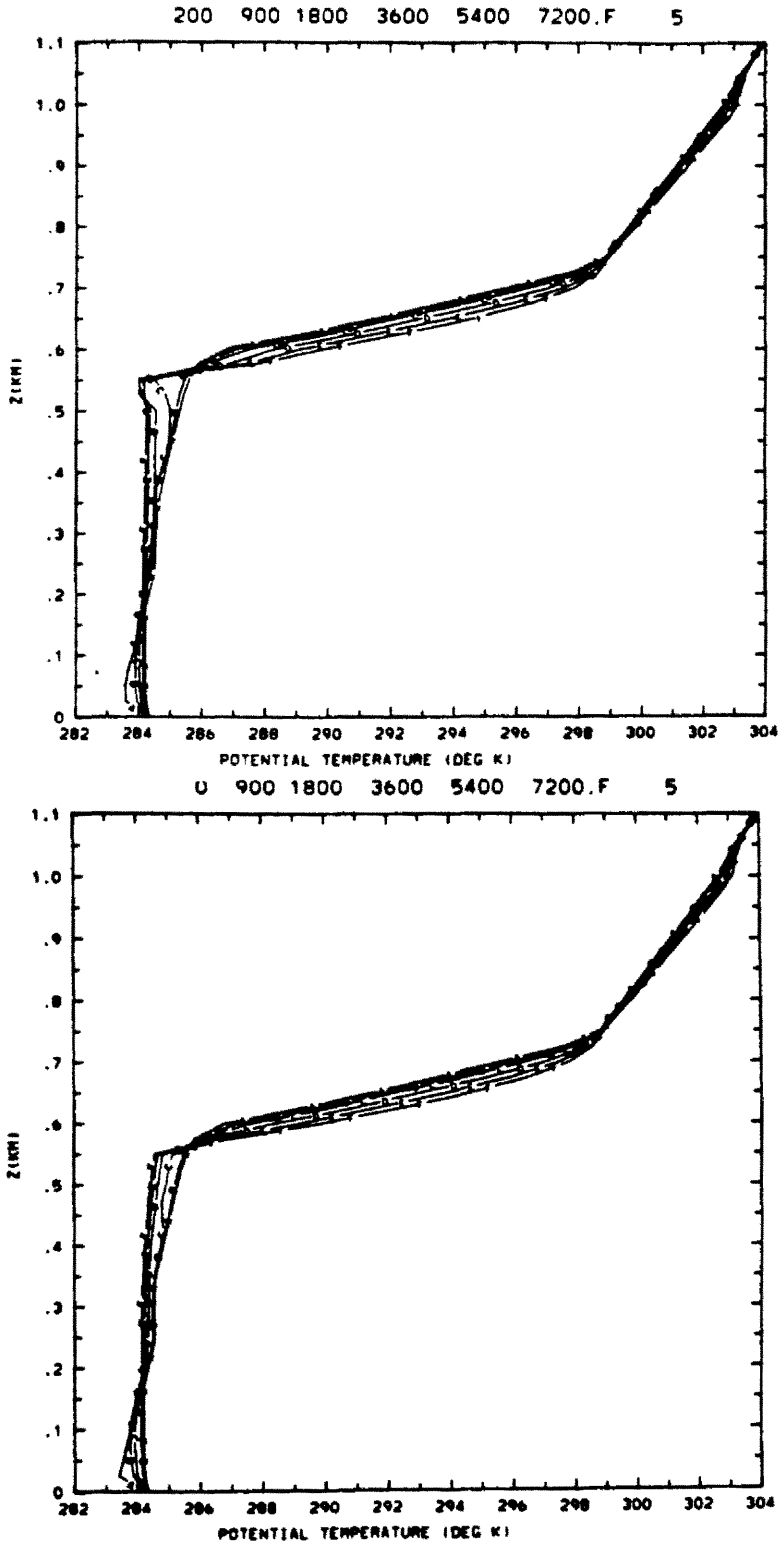

Fig. 5.7. Comparison of potential temperature vertical profile as predicted by (a) Level 2.5 model and (b) Level 4.0 model.

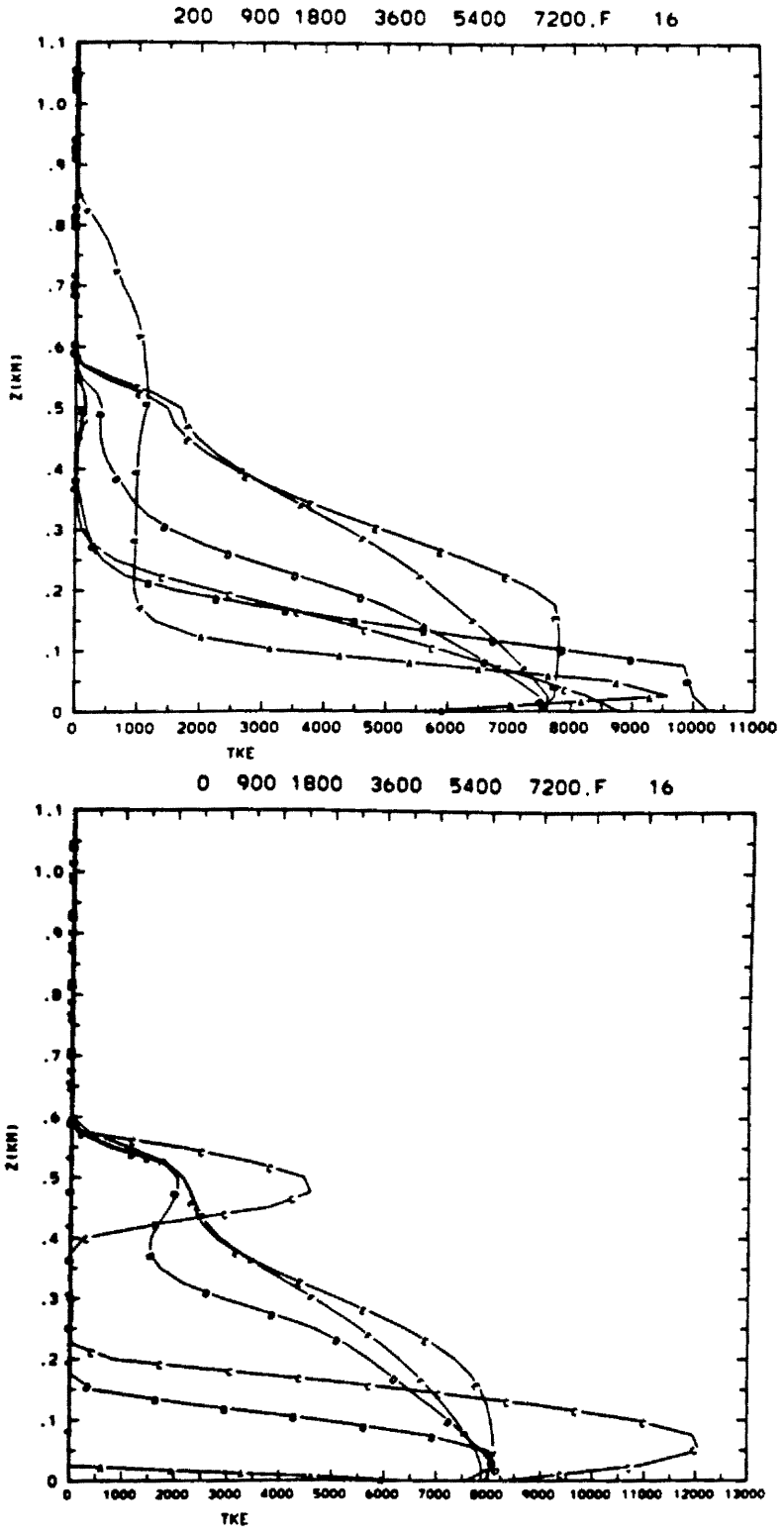

Fig. 5.8. Comparison of turbulent kinetic energy profile as predicted by (a) Level 2.5 model and (b) Level 4.0 model.

6. SUMMARY, CONCLUSIONS, AND SUGGESTIONS FOR FUTURE RESEARCH

6.1 Summary

1. Several second-order turbulence closure models were developed, analyzed and used in numerical simulations. The models ranged from the most complex Level 4.0 scheme with 21 prognostic equations to a Level 3.5 scheme of the Zeman and Lumley type, to a scheme with only one prognostic equation (Level 2.5). California stratus and Wangara Day 33 were successfully predicted by these models.
2. The detailed analysis of the Mellor and Yamada closure schemes resulted in new realizability conditions for the Level 2.5 and 3.0 models. The new conditions were applied or diagnosed in the numerical simulations.
3. Chen and Cotton's model (Zeman and Lumley type of closure) was re-run and simple turbulence statistics--eddy exchange coefficients--were generated and compared with the experimental results and the Level 2.0 closure model.
4. In the course of this study several minor points were clarified, but we did not report the results. In particular, the Manton and Cotton (1977) surface layer parameterization was compared with the new data (Panofsky and Dutton, 1984) on surface-layer turbulent variances. This resulted in accepting the Manton and Cotton version of the surface-layer parameterization. Some statistical studies (cross-correlations and power spectrum analysis) of the Chen and Cotton model were performed to investigate radiation-shear-turbulence

instability at the top of the stratocumulus layer. This study was used when interpreting some of our simplified runs of the stratocumulus case.

Below we summarize some of our recommendations with respect to usage of the simplified second-order schemes in mesoscale modelling.

6.2 Conclusions and Recommendations

1. Probably the simplest and, at the same time, the strongest recommendation is to apply the lower-level second-order schemes in accordance with their assumptions. The Mellor and Yamada hierarchy is based on small parameter scale analysis (departure from isotropy), and if this assumption is not satisfied the scheme will not work properly. Although the realizability conditions should be checked diagnostically, their application should be limited as much as possible. If the model is consistently not realizeable, the only reasonable solution is to implement the higher level scheme. If the non-realizeable solutions occur sporadically (model spin-up time, transition from day to night, top of the PBL), and if the main emphasis of the model is not on a very detailed physical depiction of these regimes, it can be used with some confidence. We think that modifying the model constants only on the basis of the model's poor predictive value should be undertaken with caution. For example, recently Grandin (1984) used a Level 2.5 model to study fog development at Cabauw. Because the model results were not consistent with the experimental data, he adjusted the model constants and introduced different parameters for regions where condensation occurs. This concept should be further analyzed because not much is known about turbulence in the cloudy region, but

the analysis of model assumptions and possible usage of the higher level scheme could be useful.

2. When one studies the details of physical mechanisms governing the flow, the higher level scheme should be used. A good example (but in a sense a negative one) is the result presented in Chapter 5 of this thesis. We used the Level 2.5 scheme to study the stratocumulus cloud. The results showed good agreement with the experiment's mean flow profiles and entrainment fluxes. On the other hand, Chen (1984) predicted that at the top of the stratocumulus layer transients in the mean flow may occur due to radiation-shear-turbulent interaction. This leads to rapid departure from the local equilibrium assumption. The diffusional terms play an important role in the buoyancy distribution. But in the Level 2.5, diffusional terms are scaled out except in the TKE equation.

3. Recently Yamada (1983) and Bader (1985) used a hybrid model with predictive TKE but with the Level 2.0 functions diagnosing eddy exchange coefficients S_M and S_H. Such a hybrid model is overspecified in the sense that the local equilibrium assumptions give (diagnostically) values of TKE which are, at the same time, predicted. This may result in non-realizable (negative) velocity variances because the local equilibrium hypothesis is used to simplify the diagnostic variance equations (Yamada, 1975). Such a model allows for TKE advection but should be used with care for the study of pollution transport in a detailed simulation of flow in a mountainous region.

6.3 Suggestions for Future Research

1. The second-order closure should be further applied to study details of various physical mechanisms interacting and producing mixed layers. In particular, more physical mechanisms could be taken into account. Some of the extensions include:
   a) The role of rainfall in the stratocumulus clouds--this was observed to be important in the developement of the North Sea stratocumulus (Nicholls,1984, 1985; Brost, 1982) case.
   b) Study of ice-turbulence-radiation interaction - this is important, for example, in the dynamics of large cumulonimbus anvil and altostratus (Sue Chen, personal communication).
   c) The cirrus dynamics are shown to be highly turbulent, with radiation playing an important destabilizing role (Starr, 1982). It is surprising that a second-order closure model has not been applied to to this problem. The only theoretical study known to the author is Starr's 2D large eddy model.
2. The diurnal behavior of the details of the PBL could be studied by the second-order closure technique. In fact it is the only feasible method now to perform such a study when a simple mixed layer model fails. Bougeault (1985) was able to predict the structure of the two-layer North Sea stratus with the third-order closure scheme without any substantial changes to it. Nicholls (1985a,b) was forced to modify the mixed layer approach and to introduce two layers to obtain agreement with the experiment. It would be challenging to perform a study similar to that of Bougeault but with the simplified second-order closure models. Also, such a study could be

extended to investigate the diurnal behaviour of the PBL in other regional and seasonal meteorological conditions.

3. One of the most celebrated problems in Sc dynamics--the entrainment mechanisms at the top of the cloud--is still controversial. Randall's (Randall, 1980 and 1984; Randall and Suarez, 1984) criteria - LCI (layer cloud instability), CDE (cloud deepening through entrainment) and TCI (thin cloud instability) are possible objects of study in higher-order closure models: however, the adequacy of a Level 2.5 model for this purpose is doubtful.
4. The second-order model closure could be used to study the sensitivity of PBL predictions (height of the mixed layer, mean profiles) to the external forcings (bottom heat flux, lower tropospheric lapse rate, vertical motion). This is an important problem in mesoscale and GCM modeling related to finding modus vivendi between sophistication of parameterization and errors in physics initialization (see more about this in Driedonks, 1985).

BIBLIOGRAPHY

Albrecht, B., R. Penc and W.H. Schubert, 1985: An observational study of cloud-topped mixed layers, J.Atmos.Sci., 42, 800-822.

Bader, D.C., 1985: Regional boundary layer evolution in mountainous terrain. Ph.D. Thesis, Dept. of Atmospheric Science, Colorado State University, Fort Collins, CO, 80523.

Banta, R. and W.R. Cotton, 1980: On computing average cloud-water quantities in a partially cloudy region. J. de Rech. Atmos., 14, 487-492.

Bougeault, Ph., 1985: The diurnal cycle of the marine stratocumulus layer: a higher-order model study, Submitted to the J.Atmos.Sci.

Brost, R.A., D.H. Lenschow and J.C. Wyngaard, 1982a: Marine stratocumulus layers. Part I: Mean conditions. J. Atmos. Sci., 39, 800-817.

Brost, R.A., J.C. Wyngaard, D.H. Lenschow, 1982b: Marine stratocumulus layers. Part II: Turbulence budgets. J. Atmos. Sci., 39, 818-836.

Businger, J.A., Wyngaard, J.C., Izumi, Y., and Bradley, E.F., 1971: Flux-Profile Relationship in the Atmospheric Surface Layer, J. Atmos. Sci., 28, 181-189.

Chen, C. and W.R. Cotton, 1982: The physics of marine stratocumulus clouds. Cloud Physics Conference, Nov. 15-18, 1982, Chicago, IL, AMS.

Chen, C., and W.R. Cotton, 1983a: A one-dimensional simulation of the stratocumulus-capped mixed layer. Boundary-Layer Meteorol., 25, 289-321.

Chen, C., and W.R. Cotton, 1983b: Numerical experiments with a one-dimensional higher-order turbulence model: Simulation of the Wangara Day 33 Case. Boundary-Layer Meteorol., 25, 375-404.

Chen, C., 1984: The physics of the marine stratocumulus-capped mixed layer, Ph.D Thesis, Colorado State University, Fort Collins, Colo.

Driedonks, A.G.M., 1985.: Modeling and Observations of the Stratocumulus-topped Atmospheric Boundary Layer, Report prepared for WMO/CAS Group of rapporteurs on Atmospheric Boundary Layer Problems.

Enger,L., 1983, Numerical boundary layer modeling with application to diffusion, Part 1: A two-dimensional higher-order closure model, Department of Meteorology, University of Uppsala, Sweden, Report No 70.

Grandin, G., 1984: Studies of the PBL with a one-dimensional model including surface energy balance, Department of Meteorology, University of Uppsala, Sweden, Report # 78, Uppsala.

Hassid, S. and B.Galperin, 1983: A turbulent energy model for geophysical flows, Boundary-Layer Meteorol., 26, 397-412.

Hearn, A.C., 1984: REDUCE User's Manual, Ver. 3.0, The RAND Corp., Santa Monica, Rand Publ. CP78(4/83).

Helfand, H.M. and J.C.Labraga, 1985: Design of a nonsingular Level 2.5 second-order closure model for the prediction of atmospheric turbulence, submitted for publication.

Herman, G. and R. Goody, 1976: Formation and persistence of summertime arctic startus cluds, J.Atmos.Sci., 33, 1537-1553.

Komori,S., H. Ueda, F. Ogino and T. Mizushina, 1982: Turbulence structure in unsteady-stratified open-channel flow, Phys.Fluids, 25, 1539-1546.

Lacis, A.A., and J.Hansen, 1974: A parameterization for the absorption of solar radiation in earth's atmosphere. J.Atmos.Sci., 31, 118-133.

Louis, J-F.,1979: A parametric model of vertical eddy fluxes in the atmosphere, Boundary-Layer Meteorol., 17, 187-202.

Manton, M.J. and W.R. Cotton, 1977: Parameterization of the Atmospheric Surface Layer, J. Atmos. Sci., 34, 331-334.

Mellor, G.L., 1973: Analytic prediction of the properties of stratified planetary surface layers, J.Atmos.Sci., 30, 1061-1069.

Mellor, G.L., 1977: The Gaussian Cloud Model relations. J. Atmos. Sci., 34, 356-358 and 1483-1484.

Mellor, G.L., and T. Yamada, 1974: A hierarchy of turbulence closure models for planetary boundary layers, J.Atmos.Sci., 34, 1791-1806. (Corrigenda, J.Atmos.Sci., 34, 1482, 1977).

Mellor, G.L., and T. Yamada, 1982: Development of a Turbulence Closure Model for Geophysical Fluid Problems, Rev.Geophys.Space Phys., 20, 851-875.

Nicholls, S., 1984: The dynamics of stratocumulus: aircraft observations and comparisons with a mixed layer model, Quart.J.R.Met.Soc., 110, 783-820.

Nicholls, S., and J. Leighton, 1985: An observational study of the structure of stratiform cloud sheets. Part I and Part II, to be published.

Panofsky, H.A. and J.A.Dutton, 1984: Atmospheric Turbulence, Models and Methods for Engineering Applications, Wiley, New York.

Randall, D.A., 1980: Conditional instability of the first kind upside-down. J. Atmos. Sci., 37, 125-130.

Randall, D.A., 1984: Stratocumulus cloud deepening through entrainment, Tellus, 36A, 446-457.

Randall, D.A. and M.J.Suarez, 1984: On the dynamics of stratocumulus formation and dissipation, J.Atmos.Sci., 41, 3052-3057.

Rodgers, C.D., 1967: The use of emissivity in atmospheric radiation calculations. Quart. J. Roy. Meteor. Soc., 93, 43-54.

Rotta, J.C., 1951: Statistische Theorie Nichthomogener Turbulentz, Z.Phys., 129, 547-572.

Starr, D.O'C., 1982: Numerical experiments on the formation and meintenance of cirriform clouds, Ph.D dissertation, Colorado State University, Fort Collins, Colo.

Stephens, G.L., 1977: The transfer of radiation in cloudy atmosphere. Ph.D. Thesis. Meteorology Department, University of Melbourne.

Stephens, G.L., 1978a: Radiation profiles in extended water clouds. I: Theory. J. Atmos. Sci., 35, 2111-2122.

Stephens, G.L., 1978b: Radiation profiles in extended water clouds. II: Parameterization schemes. J. Atmos. Sci., 35, 2123-2132.

Stephens, G.L. and Webster, P.J., 1979: Sensitivity of radiative forcing to variable clouds and moisture. J. Atmos. Sci., 36, 1542-1556.

Tripoli, G.J., and W.R. Cotton, 1982: The Colorado State University three-dimensional cloud/mesoscale model - 1981. Part I: General theoretical framework and sensitivity experiments. J. de Rech. Atmos., 16, 185-220.

Ueda,H., S.Mitsumoto and S.Komori, 1981: Buoyancy effects on the turbulent transport processes in the lower atmosphere, Quart. J. Roy. Meteor. Soc., 107, 561-578.

Weber, A.H., J.S. Irwin, J.P. Kahler., and W.B. Petersen, 1975: Atmospheric turbulence properties in the lowest 300 meters, Environmental Monitoring Series, U.S. Environmental Protection Agency, EPA-600/4-75-004.

Yamada, T., 1975: The critical richardson number and the ratio of the eddy transport coefficients obtained from a turbulence closure model, J. Atmos. Sci., 32, 926-933.

Yamada, T., 1978: A three-dimensional, second-order closure numerical model of mesoscale circulation in the lower atmosphere, Topical Rep. ANL/RER-78-1, 67pp., Radiol. and Environ. Res. Div., Argonne Natl. Lab., Argonne, Ill.

Yamada, T., and G.L. Mellor, 1975: A simulation of the Wangara atmospheric boundary layer data, J.Atmos.Sci., 32, 2309-2329.

Yamada, T. and G.L. Mellor, 1979: A numerical simulation of the BOMEX data using a turbulence closure model coupled with ensemble cloud relations, Q.J.Roy.Meteorol.Soc., 105, 915-944.

Yamada, T., 1983: Simulations of nocturnal drainage flows ba a q^2 l turbulence model, J. Atmos. Sci., 40, 91-106.

Zeman, O. and J.L. Lumley, 1976: Modeling buoyancy driven mixed layers. J. Atmos. Sci., 33, 1974-1988.

Zeman, O. 1975: The dynamics of entrainment in the planetary boundary layer: A study in turbulence modeling and parameterization. The Pennsylvania State University, Dept. Aerospace Engineering.

APPENDIX A - COMPARISON OF THE ZEMAN AND LUMLEY AND MELLOR AND YAMADA SCHEME

"Given seven constants, I can produce an elephant on a tightrope, and with nine I can make it dance."

C.F. Gauss

In this Appendix we compare the Zeman and Lumley (1976) (ZL) and Mellor and Yamada (1982) (M-Y) second-order turbulence closure approach. It is mainly done for the purpose of continuity--previously Chen and Cotton (1983a,b) (CC) from our CSU group used ZL closure, and some research in this thesis is based on their approach. For example, Chapter 3 uses CC model to compare it with the level 2 M-Y scheme. It thus became necessary in the initial stages of this research to compare the M-Y and ZL approaches. We show here that constants describing turbulence models derived by ZL and M-Y are similar. We hope that this Appendix provides a smooth transition from the CC model to the one used extensively in this thesis.

Examination of ZL and M-Y parameterization of pressure-velocity, dissipation, and return-to-isotropy terms leads to the relationships shown in Table A1.

Table A1. Comparison between ZL and M-Y parameterization

	l_1	Λ_1	l_2	Λ_2
Mellor(1982)	$A_1 l$	$B_1 l$	$A_2 l$	$B_2 l$
Zeman(1975)	$1/3\gamma\ \mu/C_1\ l$	$1/\gamma\ l$	$1/3\gamma\ \mu/C_\theta\ l$	$1/2\gamma\ l$

l_1 - Return to isotropy length scale (stress equation)

Λ_1 - Dissipation length scale (stress equation)

l_2 - Return to isotropy length (velocity-temperature covariance)

Λ_2 - Dissipation length scale (velocity-temperature covariance)

Both ZL and M-Y assume that all length scales are proportional to each other. Therefore they set

$$(l_1, \Lambda_1, l_2, \Lambda_2) = (A_1, B_1, A_2, B_2)l \qquad \text{(A1.1)}$$

where l is the master turbulent length scale.

It can be seen from Table A1 that M-Y constants (A_1, B_1, A_2, B_2) are related to ZL constants (C_1, C_θ, μ and γ) by the following equations $A_1 = \frac{1}{3\gamma}\frac{\mu}{C_1}$, $B_1 = \frac{1}{\gamma}$, $A_2 = \frac{1}{3\gamma}\frac{\mu}{C_\theta}$ and $B_2 = \frac{1}{2\gamma}$.

ZL obtained from the experimental results $\frac{C_1}{\mu} = 3.25$ and $\frac{C_\theta}{\mu} = 7$, CC assumes $\gamma = \frac{1}{15}$. M-Y constants were carefully derived by comparison with various turbulent flows and are defined, for example, in the 1982 paper.

Table A2 presents comparison of numerical constants for ZL and M-Y scheme.

Table A2. Critical value of the flux Richardson number - R_{fc} and empirical constants used in ZL and ML models (M-Y data from Mellor and Yamada 1982, ZL data from Zeman (1975))

Author	R_{fc}	Empirical Constants						
		A_1	B_1	A_2	B_2	C_1	C_2	C_3
Mellor(1982)	0.19	0.92	16.6	0.74	10.1	0.08	0	0
Zeman(1975)		10.5/15	15	5/7	15/2	0	3/10	0

APPENDIX B - BASIC SET OF EQUATIONS FOR THE SECOND-ORDER TURBULENCE CLOSURE

B1. Level 4 - Basic Equations of Second-Order Closure

The Reynolds-averaged equations for the Reynolds stress can be written as

$$\frac{\partial \overline{u_i u_k}}{\partial t} = P_{ik} + G_{ik} + S_{ik} - \Pi_{ik} - D_{ik}, \tag{B1.1}$$

where

$$P_{ik} = -\overline{u_i u_j}\,\bar{U}_{k,j} - \overline{u_k u_j}\,\bar{U}_{i,j} \tag{B1.2}$$

and

$$G_{ik} = -\frac{g}{\rho_o}(\overline{\rho_k u_i} + \overline{\rho_i u_k}) \tag{B1.3}$$

represent the mechanical production of $\overline{u_i u_k}$ by the vertical shear of $\bar{U}_i$ and the buoyancy production terms, respectively. Somewhat unusual notation for the density is used: $(\rho_1, \rho_2, \rho_3) = (0, 0, \rho)$. The third-order correlation terms have been divided into the diffusive transport term

$$S_{ik} = -\left(\overline{u_i u_k u_j} + \frac{2}{3}\frac{\delta_{ik}}{\rho_o}\overline{p u_j}\right)_{,j} \tag{B1.4}$$

and the pressure-velocity correlation term

$$\Pi_{ik} = \frac{1}{\rho_o}\left(\overline{p_{,i} u_k} + \overline{p_{,k} u_i} - \frac{2}{3}\delta_{ik}\left(\overline{p u_j}_{,j}\right)\right). \tag{B1.5}$$

The dissipation term is given by

$$D_{ik} = \frac{2}{3}\delta_{ik}\varepsilon . \tag{B1.6}$$

The equation for the turbulent covariances of thermodynamic quantities such as $\overline{\theta_{il}}$, $\overline{r}$ and $\overline{r_r}$ with the velocity components is

$$\frac{\partial \overline{u_i a}}{\partial t} = A_{ia} + P_{ia} + G_{ia} + S_{ia} - \Pi_{ia} + PA(\overline{wa}) + S(\overline{wa}) \tag{B1.7}$$

where

$$A_{ia} = - \overline{u_j}(\overline{u_i a})_{,j} \tag{B1.8}$$

$$P_{ia} = - \overline{u_j a}\,\overline{U}_{i,j} - \overline{u_i u_j}\,\overline{a}_{,j} \ , \tag{B1.9}$$

$$G_{ia} = - \frac{g}{\rho_o}\overline{\rho a} \ , \tag{B1.10}$$

$$S_{ia} = - (\overline{u_i u_j a})_{,j} \ , \tag{B1.11}$$

$$\Pi_{ia} = \frac{1}{\rho_o}\overline{p_{,i}\, a} \ , \tag{B1.12}$$

and $PA(\overline{u_i a})$, $S(\overline{u_i a})$ are rain/cloud water terms.
The viscous distraction term has been ignored. Note that for a one-dimensional model only, derivatives (sometimes denoted by a comma) with respect to z are non-zero. The Coriolis force has been neglected.

The equation for the turbulent covariances of two thermodynamic quantities is given by

$$\frac{\partial \overline{ab}}{\partial t} = A_{ab} + P_{ab} + S_{ab} - D_{ab} + PA(\overline{ab}) + S(\overline{ab}) \tag{B1.13}$$

where

$$A_{ab} = - \overline{u_j} \, (\overline{ab})_{,j} \tag{B1.14}$$

$$P_{ab} = - \overline{u_j a} \, \overline{b}_{,j} - \overline{u_j b} \, \overline{a}_{,j} \tag{B1.15}$$

$$S_{ab} = - (\overline{u_j ab})_{,j} \tag{B1.16}$$

$$D_{ab} = 2\varepsilon_{ab} = 2q\frac{\overline{ab}}{\Lambda_2} \tag{B1.17}$$

and $PA(\overline{ab})$ and $S(\overline{ab})$ are related to the rain/cloud conversion processes. The pressure-strain term is divided into three parts, the return-to-isotropy term (Rotta, 1951)

$$\Pi_{ik}^{I} = - \frac{q}{3l_1} \left(\overline{u_i u_k} - \frac{2}{3}\delta_{ik}q^2\right) = - \frac{q}{3l_1} a_{ik} q^2 \, , \tag{B1.18}$$

shear term

$$\Pi_{ik}^{S} = C_1 q^2 \left(\frac{\partial \overline{U_i}}{\partial x_k} + \frac{\partial \overline{U_k}}{\partial x_i}\right) , \tag{B1.19}$$

and buoyancy term

$$\Pi_{ik}^{B} = C_2 \left(G_{ik} - \frac{2}{3}\delta_{ik}P_b\right) \tag{B1.20}$$

where

$$P_b = \frac{1}{2}G_{ii} = - \frac{g}{\rho_o}\overline{\rho_i u_i} \, . \tag{B1.21}$$

The departure from isotropy tensor is defined as

$$a_{ik} = \frac{\overline{u_i u_k}}{q^2} - \frac{1}{3}\,\delta_{ik} \, . \tag{B1.22}$$

The pressure term $\Pi_{1\alpha}$ is modeled as

$$\Pi_{i\alpha} = -\frac{q}{3l_2}\overline{u_i\alpha}. \tag{B1.23}$$

The dissipation is modeled according to

$$2\mu\overline{u_{i,j}u_{k,j}} = \frac{2}{3}\varepsilon\delta_{ik} = \frac{2q^3}{3\Lambda_1}\delta_{ik} \tag{B1.24}$$

i.e.,

$$\varepsilon = \frac{q^3}{\Lambda_1} \tag{B1.25}$$

and

$$2\beta\overline{\alpha_{,j}\alpha_{,j}} = 2\frac{q}{\Lambda_2}\overline{\alpha^2} \tag{B1.26}$$

i.e.,

$$\varepsilon_{aa} = \frac{q}{\Lambda_2}\overline{\alpha^2}. \tag{B1.27}$$

The length scales l_1, Λ_1, l_2, Λ_2 are proportional to each other, $(l_1, \Lambda_1, l_2, \Lambda_2) = (A_1, B_1, A_2, B_2)\, l$, and A_1, B_1, A_2, B_2 are defined by Eq. (A1.1).

The turbulent kinetic energy (TKE) equation can be formed using (B1.1). Thus,

$$\frac{\partial}{\partial t}q^2 = P_{ii} + G_{ii} + S_{ii} - \Pi_{ii} - D_{ii}. \tag{B1.28}$$

If we let

$$P_s = \frac{1}{2}P_{ii} \tag{B1.29}$$

and

$$P_b = \frac{1}{2}G_{ii}, \tag{B1.30}$$

we have $D_{ii} = 2\varepsilon$ and the Π_{ii} tensor is trace-free, then

$$\frac{\partial}{\partial t}q^2 = 2\,(P_b + P_s - \varepsilon) + S_{ii}. \qquad \text{(B1.31)}$$

Multiplying the TKE equation by $\frac{\delta_{ik}}{3}$ we obtain

$$\frac{d}{dt}\frac{\delta_{ik}}{3}q^2 = \frac{2}{3}\delta_{ik}\,(P_b + P_s - \varepsilon) + \frac{\delta_{ik}}{3}S_{ii}. \qquad \text{(B1.32)}$$

We can form the prognostic equation for the departure from isotropy tensor

$$\frac{d}{dt}a_{ik}q^2 = (P_{ik} - \frac{2}{3}\delta_{ik}P_s) + (G_{ik} - \frac{2}{3}\delta_{ik}P_b) + (S_{ik} - \frac{\delta_{ik}}{3}S_{ii})$$

$$- \frac{q}{3l_1}a_{ik}q^2 + C_2(G_{ik} - \frac{2}{3}\delta_{ik}\,P_b). \qquad \text{(B1.33)}$$

Notice that the dissipation term canceled out, but we did not assume the local equilibrium, i.e., $P_s + P_b = \varepsilon$.

B2. Level 3.0 and 2.5 Approximations

Mellor and Yamada (1974) performed analysis of Eq. (B1.1,7,33) in terms of small parameter a_{ik} . They showed that one can neglect time derivatives and the triple correlation terms; i.e., we can write

$$\frac{q}{3l_1}\,a_{ik}\,q^2 = (P_{ik} - \frac{2}{3}\delta_{ik}\,P_s) + C_{21}(G_{ik} - \frac{2}{3}\delta_{ik}\,P_b) \qquad \text{(B2.1)}$$

where $C_{21} = 1 + C_2$.

For turbulent covariances with thermodynamic quantities we have, after neglecting time derivatives, advection, triple correlation, PA and S terms

$$-\frac{q}{3l_2}\overline{u_i\alpha} = P_{i\alpha} + G_{i\alpha} \qquad \text{(B2.2)}$$

$$2\frac{q}{\Lambda_2}\overline{ab} = P_{aa}. \qquad \text{(B2.3)}$$

Level 3.0 equations can be written in the component form (compare with Yamada, 1978 and Yamada and Mellor, 1979)

$$\overline{u^2} = \frac{q^2}{3} + \frac{l_1}{q}\left[-4\,\overline{uw}\,\frac{\partial \bar{U}}{\partial z} + 2\,\overline{vw}\,\frac{\partial \bar{V}}{\partial z} - 2\,C_{21}\,P_b\right]$$

$$\overline{v^2} = \frac{q^2}{3} + \frac{l_1}{q}\left[2\,\overline{uw}\,\frac{\partial \bar{U}}{\partial z} - 4\,\overline{vw}\,\frac{\partial \bar{V}}{\partial z} - 2\,C_{21}\,P_b\right]$$

$$\overline{w^2} = \frac{q^2}{3} + \frac{l_1}{q}\left[2\,\overline{uw}\,\frac{\partial \bar{U}}{\partial z} + 2\,\overline{vw}\,\frac{\partial \bar{V}}{\partial z} + 4\,C_{21}\,P_b\right] \qquad \text{(B2.4a,b,c)}$$

$$-\overline{uv} = \frac{3l_1}{q}\left[\,\overline{uw}\,\frac{\partial \bar{V}}{\partial z} + \overline{vw}\,\frac{\partial \bar{U}}{\partial z}\,\right]$$

$$-\overline{uw} = \frac{3l_1}{q}\left[\,\overline{(w^2 - C_1 q^2)}\,\frac{\partial \bar{U}}{\partial z} - C_{21}\,\frac{g}{\rho_o}\,\overline{\rho u}\,\right]$$

$$-\overline{vw} = \frac{3l_1}{q}\left[\,\overline{(w^2 - C_1 q^2)}\,\frac{\partial \bar{V}}{\partial z} - C_{21}\,\frac{g}{\rho_o}\,\overline{\rho v}\,\right] \qquad \text{(B2.5a,b,c)}$$

$$-\overline{u\theta_{il}} = \frac{3l_2}{q}\left[\overline{uw}\,\frac{\partial \overline{\theta_{il}}}{\partial z} + \overline{w\theta_{il}}\,\frac{\partial \bar{U}}{\partial z}\,\right]$$

$$-\overline{v\theta_{il}} = \frac{3l_2}{q}\left[\overline{vw}\,\frac{\partial \overline{\theta_{il}}}{\partial z} + \overline{w\theta_{il}}\,\frac{\partial \bar{V}}{\partial z}\,\right]$$

$$-\overline{w\theta_{il}} = \frac{3l_2}{q}\left[\overline{w^2}\,\frac{\partial \overline{\theta_{il}}}{\partial z} + \frac{g}{\rho_o}\overline{\rho\theta_{il}}\,\right] \qquad \text{(B2.6a,b,c)}$$

$$-\overline{ur} = \frac{3l_2}{q}\left[\overline{uw}\,\frac{\partial \bar{r}}{\partial z} + \overline{rw}\frac{\partial \bar{U}}{\partial z}\right]$$

$$-\overline{vr} = \frac{3l_2}{q}\left[\overline{uw}\,\frac{\partial \bar{r}}{\partial z} + \overline{rw}\frac{\partial \bar{V}}{\partial z}\right]$$

$$-\overline{rw} = \frac{3l_2}{q}\left[\,\overline{w^2}\,\frac{\partial \bar{r}}{\partial z} + \frac{g}{\rho_o}\,\overline{\rho w}\,\right] \qquad \text{(B2.7a,b,c)}$$

$$-\overline{ur_r} = \frac{3l_2}{q}\left[\overline{uw}\,\frac{\partial \overline{r_r}}{\partial z} + \overline{r_r w}\frac{\partial \bar{U}}{\partial z}\,\right]$$

$$-\overline{vr_r} = \frac{3l_2}{q}\left[\overline{uw}\,\frac{\partial \overline{r_r}}{\partial z} + \overline{r_r w}\frac{\partial \bar{V}}{\partial z}\,\right]$$

$$-\overline{r_r w} = \frac{3l_2}{q}\left[\overline{w^2}\,\frac{\partial \overline{r_r}}{\partial z} + \frac{g}{\rho_o}\,\overline{\rho w}\,\right] \qquad \text{(B2.8a,b,c)}$$

$$\overline{\theta_{il}^2} = -\frac{\Lambda_2}{q}\,\overline{w\theta_{il}}\,\frac{\partial \overline{\theta_{il}}}{\partial z}$$

$$\overline{r^2} = -\frac{\Lambda_2}{q}\,\overline{wr}\,\frac{\partial \bar{r}}{\partial z}$$

$$\overline{r_r^2} = -\frac{\Lambda_2}{q}\,\overline{wr_r}\,\frac{\partial \overline{r_r}}{\partial z} \qquad \text{(B2.9a,b,c)}$$

$$-\overline{\theta_{il} r} = \frac{\Lambda_2}{2q}\left(\overline{\theta_{il} w}\,\frac{\partial \bar{r}}{\partial z} + \overline{rw}\,\frac{\partial \theta_{il}}{\partial z}\right)$$

$$-\overline{\theta_{il} r_r} = \frac{\Lambda_2}{2q}\left(\overline{\theta_{il} w}\,\frac{\partial \overline{r_r}}{\partial z} + \overline{r_r w}\,\frac{\partial \theta_{il}}{\partial z}\right) \qquad \text{(B2.10a,b)}$$